Physics of the Earth and Planetary Interiors 220 (2013) 50–72

Contents lists available at SciVerse ScienceDirect

Physics of the Earth and Planetary Interiors

journal homepage: www.elsevier.com/locate/pepi

Thermal and compositional evolution of the martian mantle: Effects of water

Thomas Ruedas [a,*], Paul J. Tackley [b], Sean C. Solomon [a]

[a] Department of Terrestrial Magnetism, Carnegie Institution of Washington, 5241 Broad Branch Road, NW, Washington, DC 20015, USA
[b] Institute of Geophysics, ETH Zürich, NO H9.1, Sonneggstrasse 5, 8092 Zürich, Switzerland

ARTICLE INFO

Article history:
Received 18 April 2012
Received in revised form 14 February 2013
Accepted 20 April 2013
Available online 2 May 2013
Edited by Mark Jellinek

Keywords:
Mars
Mantle convection
Water
Rheology

ABSTRACT

We present numerical models of the thermochemical evolution of the mantle of Mars with particular attention paid to the effects of water. With a two-dimensional, anelastic, compressible convection algorithm in combination with a parameterized model of composition and thermoelastic properties, we consider how water in nominally anhydrous minerals may have influenced the melting and rheology of the martian mantle and how it may have been redistributed by melting, melt extraction, and convection over a period of 4 Gy. The strongest effect of water is found to be a marked increase in convective vigor due to the lower viscosity, which leads to faster cooling of the mantle but nonetheless enhances melt production. Modeling results are compared with observations and independent inferences from spacecraft observations and martian meteorite analyses. Some models with radionuclide concentrations from Wänke and Dreibus (1994), but with initial mantle water concentrations between their estimate of 36 ppm by weight and 10 times this value, combined with ~50% degassing of crust-forming material, partly match observed crustal concentrations of K, Th, and water. In order to account for the observed chemical variation in crustal rocks, however, the formation and survival of ancient mantle heterogeneities appears to have been necessary. Water loss from the mantle since the end of the magma ocean stage has been minor. Elevated water contents notwithstanding, the depth variation of viscosity in the sublithospheric mantle of a given model is likely minor. Depths to the Curie temperature at the end of the Noachian range from ~40 to 60 km for magnetite and hematite in the models, and present-day total crustal thicknesses lie between 75 and 100 km. The depth to the brittle–ductile transition increases from values around 30 km in the early stages of the models to 170–240 km at present. An estimate of total core entropy renders the existence of a basal perovskite + ferropericlase layer unlikely. The absence of stable superplumes in all of our preferred models suggests that the volcanic provinces of Tharsis and Elysium were formed by a succession of more short-lived events, such as transient plumes, from specific regions at the core–mantle boundary.

1. Introduction

In a companion contribution (Ruedas et al., 2013, hereafter cited as RTS1), we presented models of convection and melting in the martian mantle that incorporated details of mineralogy and thermoelastic properties, but we did not consider the effects of water on melting and rheology. In this paper, we extend those models to include water in an attempt to assess how much water was present in the early martian mantle, how much may still be remaining, and how it has influenced the evolution of the planet. As in RTS1, we also make predictions of a range of geophysical and geochemical observables and compare them with published models and observations, for instance, of crustal thickness, heat flow, chemical composition, and gravitational equipotential surface (areoid). Future missions, in particular the Interior Exploration using Seismic Investigations, Geodesy and Heat Transport (InSight) mission (e.g., Banerdt et al., 2012) that is to fly to Mars in 2016, will expand the range of observables that can, in principle, be compared with models like those of this study to include seismic observations and will improve the constraints on some of those presented here.

Laboratory investigations have shown for many years that even trace amounts of water can have major effects on rock physical properties, such as the solidus temperature versus pressure (e.g., Kushiro et al., 1968; Kushiro, 1969; Hirose and Kawamoto, 1995; Gaetani and Grove, 1998; Katz et al., 2003; Litasov and Ohtani, 2007), the rheology (e.g., Griggs and Blačić, 1965; Avé Lallemant and Carter, 1970; Karato et al., 1986; Hirth and Kohlstedt, 1996, 2003), the elastic properties, and the expected depth and vertical extent of phase transitions (Wood, 1995). Experiments on the major nominally anhydrous mantle minerals wadsleyite and ringwoo-

* Corresponding author. Tel.: +1 202 478 8846; fax: +1 202 478 8821.
E-mail address: ruedas@dtm.ciw.edu (T. Ruedas).

0031-9201/$ - see front matter © 2013 Elsevier B.V. All rights reserved.
http://dx.doi.org/10.1016/j.pepi.2013.04.006

dite have shown that they can take up much more water than olivine, their low-pressure form (Kohlstedt et al., 1996); however, it is unclear if the effect of water on the strength of these high-pressure forms is as marked as for olivine or is of only minor influence (Kubo et al., 1998; Chen et al., 1998; Karato, 2008). As noted by RTS1, the presumably more iron-rich bulk composition of Mars and its smaller size and mass give rise to a pattern of phase stability fields in the mantle different from that on Earth, one in which ringwoodite and wadsleyite occupy a much larger fractional volume. This pattern makes it conceivable, although not necessary, that much of the lower half of the martian mantle serves as a large reservoir for water or played such a role over a portion of martian history. Médard and Grove (2006) estimated that up to 0.4 wt.% water may have been buried deep in the martian mantle during accretion and that a part of that inventory may have survived later degassing events through storage in nominally anhydrous minerals. The strong effect of water on the rheology of olivine-bearing rock (e.g., Karato et al., 1986) suggests that the presence of substantial water should enable more vigorous convection, and the larger associated secular heat loss could change the style of convection markedly, judging from studies of convection in terrestrial settings (e.g., Phipps Morgan, 1997; Ito et al., 1999; Braun et al., 2000; Ruedas, 2006) and more general numerical surveys (e.g., van Thienen, 2007), but detailed studies with a full solution of the convection equations for Mars are only beginning to be conducted. Such an investigation is one of the objectives of this paper.

Several attempts have been made to estimate the water content of the martian mantle, most of them relying on geochemical arguments and analyses of martian meteorites, but the results are inconsistent. The most frequently cited studies in favor of a low water content are those by e.g., Wänke and Dreibus (1994), who arrived at an initial water concentration of 36 parts per million (ppm) by weight by considering element ratios. Moreover, they argued that oxygen isotope ratios suggest a terrestrial or a martian surface origin for that part of the water in excess of the 180 ppm found in the martian meteorite Shergotty. By contrast, Lodders et al. (1997) argued that the sequestration of Cl in the crust had not been taken into account in the element ratio calculations, and they estimated bulk Cl and water concentrations higher by a factor of 8 (McSween, 2003). This view was backed by McSween et al. (2001), who analyzed trace elements from the cores of pyroxenes in Shergotty and carried out crystallization experiments that predicted water concentrations of up to 18,000 ppm in pre-eruptive martian magmas and several hundred ppm for the mantle source. Similar results were found by McCubbin et al. (2010, 2012) from analyses of hydrous phases in the martian meteorite Chassigny and in shergottites.

The effect of water on martian mantle dynamics and evolution has been modeled only to a limited degree. The comprehensive parameterized model survey by Hauck and Phillips (2002), which focused on thermal evolution and crust formation, gave some consideration to water, among other factors, and found that the viscosity-lowering effect of water increases the growth rate and thickness of the crust compared with models with a dry mantle. Their results for a mantle with at least tens of ppm water matched observational constraints better than those for a mantle with only a few ppm water or less. The more vigorous convection in a mantle with sufficient water to alter the viscosity leads to more efficient cooling and also a thinner lithosphere at a given temperature. Hauck and Phillips (2002) estimated that no more than 5–10% of the water present in the mantle after the early degassing that accompanied planetary formation and solidification may have been lost by subsequent volcanism, because a one-plate planet degasses very inefficiently. The only full convection studies known to us that include melting and water are some preliminary results by Li and Kiefer (2007b) and Plesa and Breuer (2011) and a recent investigation by Ogawa and Yanagisawa (2012) that follows up on the paper on a water-free mantle by the same authors from 2011 and appeared while this study was under review. Li and Kiefer (2007b) modeled convection in a two-dimensional sector of the mantle in a similar phase-boundary-free setup as that of Li and Kiefer (2007a); those workers concluded that an increase in water content enhances melt production substantially, presumably more than suggested by Hauck and Phillips (2002), but they made no mention of how dehydration would affect the dynamics of the large plume featured in their model. The setup of Plesa and Breuer (2011) was a two-dimensional cross-section through the entire planet, and their model included more details of the effects of melting on physical properties and mantle dynamics. They found that dehydration and the concomitant increase in viscosity inhibit remixing of depleted mantle and that the combined effects of viscosity and melting-induced density structure reduce the extent of outgassing of the mantle. Apart from loss to the atmosphere and subsequently to space (e.g., Brain and Jakosky, 1998), it has also been suggested on the grounds of partitioning experiments that the mantle may lose water, or rather hydrogen, to the core and that the core may have absorbed an ancient martian ocean's worth of water (Shibazaki et al., 2009). Ogawa and Yanagisawa (2012) modeled martian mantle evolution in a cartesian box with aspect ratio 4 and only 1000 km depth on the grounds that the resulting surface-to-volume ratio corresponds to that of the martian mantle. Although they made an attempt to account for the high solubility of water in the high-pressure polymorphs of olivine by imposing a higher storage capability in the lower part of their model box, they did not include phase transitions in a self-consistent manner. Melt and water transport were modeled as permeable flow through the convecting solid mantle.

The presence of water would also lead to an increase in the maximum depth of melting. In terms of depth (as opposed to pressure), the shift would be larger than on Earth as a consequence of the smaller pressure gradient, as would the part of the mantle undergoing melting at any given time. Because water acts as an incompatible component during melting, it is expected that a compositional lithosphere as defined by crust plus depleted, dehydrated mantle residuum forms early and reaches a thickness of several hundred kilometers. A recent determination of the elastic lithosphere thickness of more than 300 km from Mars Reconnaissance Orbiter radar observations (Phillips et al., 2008) of lithospheric deflection by the northern polar deposits might be explained in terms of dehydration of the mantle rather than the purely thermal interpretation offered by those authors.

2. Method

Our approach combines a detailed model of thermoelastic properties of mineral assemblages that are thought to be typical for the silicate part of Mars and undergo phase transitions with a convection algorithm in the anelastic, compressible approximation. Most of the aspects of this methodology follow that by RTS1, so we give only a short summary here and refer the reader to that paper and to Tackley (1996, 2008), Tackley and King (2003), Xie and Tackley (2004), and Hernlund and Tackley (2008) for the general numerical details of the method, including the properties of the spherical annulus grid geometry and the approach to representing and tracking chemical components. The philosophy behind our approach of constructing a model that includes a very detailed representation of the planetary materials involved and their physical and chemical properties is the same as outlined by RTS1. By striving to account for reasonably well constrained properties of the planet as precisely as we can, we hope to avoid some of the arbitrariness that would be introduced in a simpler model and to facilitate a physi-

cally consistent derivation of a broad range of observables. We use the same nomenclature for the layers of the mantle identified on the basis of phase transitions in the $(Mg,Fe)_2SiO_4$ system, i.e., upper, lower, and basal layer for the depth range from the surface to the shallowest mid-mantle phase transition of olivine, downward from there to the appearance of perovskite (pv) + ferropericlase (fp), and, if applicable, for the thin (pv + fp)-containing layer at the base of the mantle, respectively (Fig. 1). In this section we focus mostly on those parts of the methodology specific to water.

As described by RTS1, the thermoelastic properties of mantle material are determined from the properties of the constituent minerals using thermodynamic data mostly from the database of Saxena et al. (1993) and thermal conductivity data from Hofmeister et al. (2007) and applying formulae from effective medium theory. For the near-surface regions, the effect of porosity on density and thermal conductivity is included via a parameterization from Leone et al. (2011). The phase relations in peridotite (Fig. 1) are for a model martian mantle rock composition (Bertka and Fei, 1997) and are described by a parameterization of experimental phase diagrams in pressure p, temperature T, and the molar ratio Mg/(Mg + Fe) = Mg#. The parameterization is based on data from Katsura and Ito (1989), Ito and Takahashi (1989), and Katsura et al. (2004) for the system $(Mg,Fe)_2SiO_4$ and on work on simplified compositions (e.g., Gasparik, 2003; Fei et al., 2004) to describe the other mineral phases. The phase relations in basaltic crustal material, specifically the position of the basalt–eclogite transition and its dependence on water content, are taken from Litasov and Ohtani (2007), but the physical properties are represented in a simpler form than those of peridotite, ensuring only that the differences in density and thermal conductivity are captured. The thermoelastic information for peridotite is also used to derive the initial adiabat and an internally consistent radial gravity profile and pressure–depth mapping. The thermal evolution of the core, which is linked to the bottom boundary conditions of the mantle, is described in a parameterized form following Nimmo et al. (2004), with a number of adjustments specific for assumed martian core material explained in detail by RTS1.

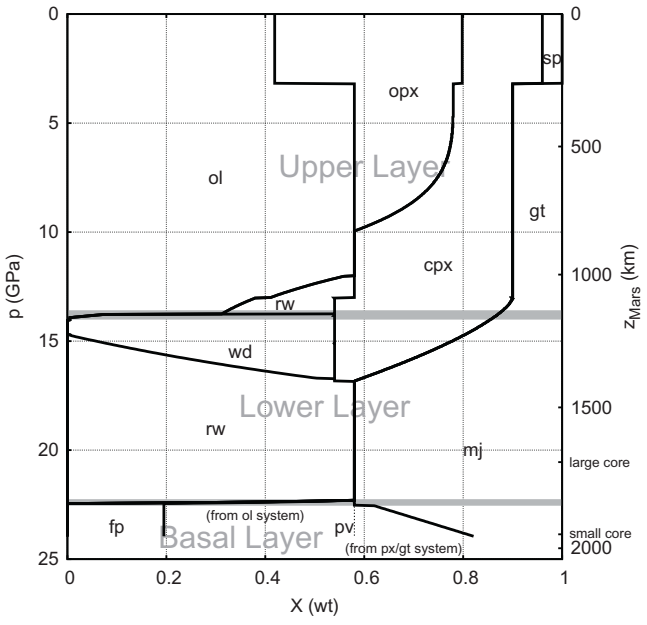

Fig. 1. Mineralogical composition for initial adiabat with a potential temperature of 1773 K for Mg# of 0.75 as calculated from the mineralogy parameterization (modified from RTS1). Mineral names are abbreviated as follows: ol – olivine, opx – orthopyroxene, cpx – clinopyroxene, sp – spinel, gt – garnet, rw – ringwoodite, wd – wadsleyite, mj – majorite, pv – perovskite, fp – ferropericlase. The approximate boundaries of the upper, lower, and basal layer as defined in the text are show in grey.

Melting degree f influences convection dynamics through compositional buoyancy and its effect on internal heating and viscosity through the content of trace components. It was tracked using the tracer ratio method (e.g., Tackley and King, 2003). If melt exceeded a threshold melt content of 1.5% (e.g., Faul, 2001), the excess was extracted instantaneously and added to the top of the crust as basaltic material, unless its density was greater than that of the matrix or stretches of subsolidus material separated it from the base of the lithosphere. The thermochemical properties of the basaltic component, which is represented by negative values of f, are not modeled at the same level of detail as those of the peridotite, but its density and viscosity were described as an anomaly of the peridotite. The generation or crystallization of melt follows the general approach of Hernlund and Tackley (2007) or Keller and Tackley (2009), but uses a more detailed parameterization of the solidus derived from experimental data (Bertka and Holloway, 1994; Schmerr et al., 2001) and of the melting degree similar to that of Katz et al. (2003). The solidus parameterization also serves to provide an estimate of the consumption or release of latent heat by melting or crystallization, respectively. The amount of melt generated or frozen follows from the difference between the advected melting degree and the one given by the parameterization, taking into account that advected melt erupts if the aforementioned conditions are met. Extracted melt removes heat from the mantle and is simply added to the surface, i.e., we neglect intrusive volcanism and its thermal consequences and assume that its heat is radiated away, because good constraints on these processes are lacking. The impact of such simplifications has been discussed by Keller and Tackley (2009), who did not find them to be of major importance to their models, and the high eruption efficiency (>80%) found by O'Neill et al. (2007) suggests that they are acceptable as an approximation.

Data on the effect of water on elastic properties of minerals are not available for several of the relevant phases, especially those stable under higher pressures, and the experimental results to date pertain mostly to density and bulk modulus, with little information on thermal expansivity, heat capacity, or thermal conductivity. Although water may affect the appropriate initial temperature profile for models of the last 4 Gy of martian thermal history, we compute the initial adiabatic profile here on the basis of dry-mineral data. Variations in the positions and depth extents of phase transitions from this assumption could be 10 km or more, but experimental data are limited to terrestrial mantle compositions or pure mineral systems (Litasov and Ohtani, 2007) rather than material with the higher iron content appropriate to the mantle of Mars. Moreover, the influences of water, iron, and the presence of other, non-transforming phases counteract one another to some extent, so on the global scale of the models presented here, and given the limited resolution of the numerical grid, the errors introduced by this simplification can be considered minor.

For internal heat sources we considered the strongly incompatible long-lived radioisotopes ^{40}K, ^{232}Th, ^{235}U, and ^{238}U, which are present in martian peridotite at similarly low concentrations as in terrestrial. Water may be present at higher concentrations than radionuclides, but its abundance in peridotite is still sufficiently low so that it may be treated as a trace component, i.e., by utilizing tracer particles to describe its transport and concentration. As in RTS1, the trace components are redistributed upon melting according to the bulk partition coefficient of the prevailing mineral assemblage, which is determined from the individual mineral partition coefficients for the radionuclides (Hauri et al., 1994; Harlow, 1997; Blundy and Wood, 2003; Mibe et al., 2006) and water (Bolfan-Casanova et al., 2000, 2003; Aubaud et al., 2004; Hauri et al.,

2006; Kohn and Grant, 2006; Grant et al., 2007) under the assumption of non-modal, nearly fractional melting in which only melt in excess of a content of 1.5% of the bulk rock is extracted. We do not allow here for the formation of hydrous minerals or water as a free phase in the mantle. The starting concentrations of water, and also of the radionuclides, are taken to be homogeneous; the complexity required to reproduce the suggestions from Médard and Grove (2006) concerning the early distribution of water lies beyond the models here, and by starting at 4 Gy before present, we assume implicitly that any hydrous phases have broken down so that their water was either lost by degassing or incorporated in lower concentrations in nominally anhydrous phases, and that any early large-scale degassing stage, which would be related to a magma ocean or perhaps to large impacts, is complete. Volcanic activity is assumed to lead to slow further degassing of the mantle. Elaborate treatments such as the parameterized dike model of O'Neill et al. (2007) are similarly beyond the scope of this paper. Instead we simply assume that a certain constant fraction of water is lost permanently to the atmosphere from all crust-forming material and will not be stored in the crust or later be recycled into the mantle, e.g., by foundering of the lower crust. This fraction is 50% in most models, but model pairs with 10% and 90% degassing, respectively, have also been run as variants of the reference case. Furthermore, we assume that no hydrogen is lost to the core, i.e., the CMB is impermeable to water; in Appendix A we show that the substantial loss of hydrogen to the core suggested by Shibazaki et al. (2009) is unlikely to have occurred.

Lowering of the solidus temperature by water is not well constrained even for the terrestrial mantle, let alone for Mars. In RTS1, the dry solidus and the liquidus were parameterized by piecewise polynomial fits in p to experimental data for a martian rock composition. Melting degree f was parameterized as a function of a p-dependent normalized temperature, specifically as a continuous sequence of concave-up curves spanning the interval between the bulk solidus and the liquidus, with kinks at points of phase exhaustion. In contrast to terrestrial peridotite, the temperature interval between the solidus and exhaustion of clinopyroxene was assumed to be narrower for Mars on the grounds of experimental data (Bertka and Holloway, 1994). The melting parameterization by Katz et al. (2003) describes the reduction as a function of the weight fraction of water in the melt of the form $\Delta T_{s,dw} = c_s C_{w,f}^{v}$, with the parameters c_s and v determined by fit to laboratory measurements. With no experimental data available to make a fit for martian compositions, we chose to set $v = 1$ as did Davies and Bickle (1991) and estimated c_s by treating martian mantle material as a pure solid with trace amounts of a solidus-lowering second component. In such a case, we have

$$\Delta T_{s,dw} = c_s C_{w,f} = \frac{R T_{s,d}^2}{L} X_{w,f} \tag{1}$$

(Hirschmann et al., 1999), where R is the molar gas constant, $X_{w,f}$ is the mole fraction of water in the melt, $T_{s,d}$ is the dry solidus, and L is the latent heat as determined from the parameterization of the dry solidus and the molar volumes of the solid and the melt as given by RTS1. Determination of the density of the hydrous melt follows Jing and Karato (2009) and uses the equation of state for water of Sakane et al. (2001). This procedure gives plausible results at least for the stability field of olivine. At the relatively low water concentrations of at most 360 ppm water in unmolten peridotite in our models, the difference in size of the melting zone between the models of this study and the dry ones of RTS1 is only minor, in agreement with what is expected from the parameterization by Katz et al. (2003) for low water contents. Therefore, the mid-mantle is still essentially solid. Moreover, extant deep melt is likely to be too dense to ascend (e.g., Agee, 2008), so such melt should remain trapped and not directly affect the evolution of shallower portions of the system. As a consequence, the trace components in such melt also remain in place and reenter the solid matrix if the trapped melt refreezes.

Apart from the solidus temperature, water in the martian mantle has the greatest effect on thermal evolution through its influence on viscosity. Except in models where the phase transition to perovskite + ferropericlase is present, olivine or one of its high-pressure forms is the volumetrically dominant phase in the mantle, especially in rock that has undergone some melting; otherwise, it is perovskite. We assume for simplicity that the dominant phase essentially controls the rheology, so that the concentration of water in that phase rather than the bulk water content has to be considered in evaluating viscosity. This effective water content is estimated from the partition coefficients: $C_{eff} = C_{blk} D_{dom}/D_{blk}$. This treatment leads to a higher viscosity than if the bulk water content were used, except in the lower layer of the mantle, where the viscosity is lower at a given C_{blk}. The viscosity depends on pressure, temperature, porosity (melt content) φ, Mg#, mineralogy X, and water content, and is determined with a rheological law following Hirth and Kohlstedt (2003) and Zhao et al., 2009:

$$\eta(p,T,\varphi,\mathrm{Mg}\#,X) = \eta_p(X)\frac{b^3}{A C_{OH}}\left(\frac{1-\mathrm{Mg}\#_{ref}}{1-\mathrm{Mg}\#}\right)^{1.5} \cdot \exp\left[\frac{E+pV+c(\mathrm{Mg}\#_{ref}-\mathrm{Mg}\#)}{RT} - a\varphi\right]. \tag{2}$$

This relation is similar to that in RTS1, but A, E, and V have different values in the presence of water; all applicable parameters are summarized in Table 1. Eq. 2 also includes a factor $1/C_{OH}$ to account for the concentration of OH^- ions, as appropriate for diffusion creep in hydrous olivine. In order to avoid a singularity for $C_{OH} \to 0$, we switch to the parameters for dry olivine given by RTS1 following Hirth and Kohlstedt (2003), under the assumption that the transition takes place when the water concentration falls below 3 ppm; this concentration corresponds approximately to the threshold of $50\mathrm{H}/10^6$ Si given for olivine by Kohlstedt et al. (2000, pp. 24–25). In RTS1, the petrological term $\eta_p(X)$ quantifying the viscosity contrast of a given mantle petrological composition X with upper-mantle peridotite was set to 2.5 and 10 for the lower and basal layers, respectively. Because of the aforementioned uncertainty about the rheological effect of water on most of the high-pressure forms of mantle minerals, we ran models with these values but also with larger $\eta_p(X)$ for the lower and the basal layer in order to reduce the drop in viscosity at the mid-mantle phase transitions separating the upper and lower layer and make it more similar to the viscosity profile of Steinberger et al. (2010). The parameters a, b, and c are kept at fixed values; a and c are taken from experimental work, and although c may be seen as preliminary given the scarcity of studies of the effect of iron on creep, the corresponding terms should have only a minor impact on the dynamics in our models.

3. Results

3.1. Model set-up

The choice of initial and boundary conditions and parameters in the models presented here follows the same principles as given by RTS1. Therefore, we have excluded the first few hundred million years of martian evolution, which were complex and influenced by processes such as multiple asteroidal or cometary impacts and possibly the overturn of crystallization products of an early magma ocean. These were important factors in Mars' early history and are thought to have a potentially substantial effect on the planform of mantle convection (e.g., Roberts and Arkani-Hamed, 2012) but cannot be modeled self-consistently with our algorithm at this

Table 1
Parameters in Eq. 2. Reference values of variable parameters are printed in italics.

A	1.5×10^9	Hirth and Kohlstedt (2003), dry diffusion, olivine
	10^6	Hirth and Kohlstedt (2003), wet diffusion, olivine
E, activation energy	375 kJ/mol	Hirth and Kohlstedt (2003), dry diffusion, olivine
	335 kJ/mol	Hirth and Kohlstedt (2003), wet diffusion, olivine
V, activation volume	6×10^{-6} m^3/mol	Hirth and Kohlstedt (2003), dry diffusion, olivine
	4×10^{-6} m^3/mol	Hirth and Kohlstedt (2003), wet diffusion, olivine
a	30	Hirth and Kohlstedt (2003)
b, grain size	1 cm	Hirth and Kohlstedt (2003)
c	38.35 kJ/mol	
$Mg\#_{ref}$	0.9	Zhao et al. (2009)
$\eta_p(X)$, "petrological factor"		
lherzolitic upper layer	1	
Basalt	0.25	After Mackwell et al. (1998)
Eclogite	1.2	After Jin et al. (2001)
Lower layer	*2.5*, 5, 15, 150	After Jin et al. (2001)
Basal layer	*10*, 15, 150	

point. In order to avoid these poorly constrained initial and boundary conditions, we chose to begin the models at 4 Ga, because at that time martian evolution likely became steadier, and the prevailing conditions can probably be estimated more reliably from available observations. As explained in RTS1, the initial crustal thickness is set by the amount of melt generated and extracted under the initial temperature conditions in the first timestep, according to the method outlined in Section 2. It should therefore lie above the estimate of 20–30 km for the earliest crust (Norman, 1999, 2002) and should not exceed the thickness of the magnetized crust of 35–55 km (e.g., Nimmo and Gilmore, 2001; Ruiz et al., 2006; Voorhies, 2008; Ravat, 2011) by much. Our simple initial conditions can be viewed as representing a hypothetical state of thorough mixing of the mantle at the end of the first ~500 My caused by the aforementioned external influences and the high mantle temperatures in the young planet. Compositionally, this assumed state would have been characterized by large-scale homogeneity if compositional heterogeneities that existed or were formed at earlier times were sufficiently small and rheologically similar to the ambient mantle (e.g., Spence et al., 1988; Manga, 1996). The extent to which present features of Mars cannot be explained by a model with such simple initial conditions indicates implicitly how well ancient features from the first 500 My may have survived later events.

As in the earlier study, we ran a large-core (LC, $r_c = 1690$ km, 36.5 wt% S) and a small-core (SC, $r_c = 1440$ km, 13.5 wt% S) version of each parameter combination, because the size of the core is still uncertain, and available data neither require nor exclude the existence of a basal pv + fp layer that would exist in the SC but not in the LC model. The Mg# of the mantle is 0.75 in all models. The pair of reference models (LC-ref and SC-ref) largely corresponds to the reference model pair of RTS1, except that the initial water concentration is set to the Wänke and Dreibus (1994) value of 36 ppm and a hydrous rheology is assumed; the petrological factors $\eta_p(X)$ for the lower and basal layers are also 2.5 and 10, respectively. In this paper, we refer to models with these standard rheological parameters as models with a "reference viscosity". An additional model pair (eL) was run with a modestly elevated lower-layer viscosity with $\eta_p(X) = 5$, and several pairs at different water concentrations or potential temperatures with a substantially higher viscosity ($\eta_p(X) = 15$) for both the lower and the basal layer (hL). A model pair (xL) with an even higher viscosity in the lower and basal layer ($\eta_p(X) = 150$) probes the effect of a marked increase of the viscosity at mid-mantle depths as proposed by Zhong and Zuber (2001) and Roberts and Zhong (2006) as a mechanism to induce degree-one convection. Furthermore, two model pairs, hLA0.2 and hLA10, were added in which the viscosity as given by Eq. 2 was multiplied by a constant factor of 0.2 or 10, respectively, everywhere in the mantle. These models were set up as variants of the hL pair rather than of the reference-viscosity pair because of the more satisfactory match of the hL radial viscosity profile with independent constraints, as discussed below. The purpose of these models is to probe the effect of variability in the pre-exponential factor A (or indeed the mineralogical composition of the mantle) and the grain size b in Eq. 2.

As in RTS1, the initial potential temperature is usually $T_{pot} = 1873$ K, but there are also two pairs with $T_{pot} = 1773$ K (Tpotl, TpotlhL). The initial excess temperature at the CMB, $T_{CMB,0}$, is 150 K in all models and is allowed to evolve according to the cooling of the core, whereas the surface is kept at 215 K at all times. For the surface porosity, the Clifford (1993) value of 20% is usually applied, except for one pair with 35% porosity at the surface (v35) to confirm the effect on surface heat flow observed by RTS1. As the focus of this paper is mantle water, we ran models with several different water contents: 36 ppm as in the original Wänke and Dreibus (1994) model; 180 ppm, which lies not only close to the value of the terrestrial MORB source (e.g., Saal et al., 2002) but also within the range of 140–250 ppm suggested by McCubbin et al. (2010) for the mantle source of the Chassigny meteorite and of 73–290 ppm derived by McCubbin et al. (2012) for the source of the shergottites (180, 180hL); and twice that value, i.e., 360 ppm as an extreme case (360, 360hL). The extent of degassing of "erupting" melt is assumed to be 50% in most models except for two pairs, in which the degassed fraction is set to 10% and 90%, respectively (dg0.1, dg0.9), in order to test the sensitivity of the results to this parameter. In all these models we use radionuclide contents after Wänke and Dreibus (1994). Although the more K-rich composition by Lodders et al. (1997) is deemed unlikely by RTS1, we include here a model pair (LF) with their radionuclide concentrations and their elevated water content of 288 ppm for completeness. An overview of the model parameters is given in Table 2.

3.2. Dynamical and thermal evolution

In all models of this paper, the combination of high initial temperatures and water with a low gravitational acceleration results in a large maximum depth of partial melting in the early martian mantle. Especially in hot plumes, melting can initially reach almost halfway to the base of the mantle in the more water-rich models. Experimental evidence suggests that erupted martian melts can originate from pressures as high as 14 GPa (Agee, 2008). Extraction of such melts from the mantle would therefore be very efficient in dehydrating the uppermost part of the mantle and would result in

Table 2
Model parameters. Default values of variable parameters are printed in italics; values marked with an asterisk apply only to the LF pair.

Planetary radius, R	3389.92 km
Total planetary mass, M	6.4185×10^{23} kg
Surface temperature	215 K
Mantle	
Mantle thickness, z_m	1700 or 1950 km
Initial potential temperature, T_{pot}	1773 or *1873* K
Initial core superheating	150 K
Surface porosity, φ_{surf}	*0.2* or 0.35
Melt extraction threshold	0.015
Bulk silicate Mars Mg#	0.75
Present-day K content	*305* or 920* ppm
Present-day Th content	56 ppb
Present-day U content	16 ppb
Initial water content	36, 180, 288*, or 360 ppm
Core	
Thermal expansion coefficient (CMB), α_c	$7.4–8.2 \times 10^{-5}$[a,b] 1/K
Average isobaric specific heat, c_{pc}	750 J/(kg K)
Thermal conductivity, k_c	~7.3–19.5[a,c] W/(m K)

[a] Varies between models and with time; see Appendix B in RTS1.
[b] Average values lie in the range $(6.39–6.85) \times 10^{-5}$/K.
[c] Extreme values; lower values apply to LC, larger values to SC models.

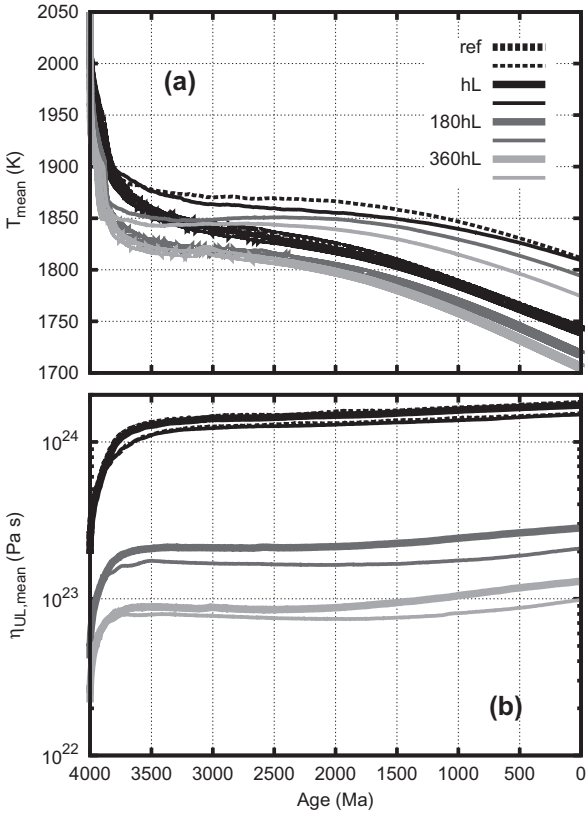

Fig. 2. Mean mantle temperature (a) and mean viscosity of the upper layer (b) as a function of time for selected models. Thick lines designate models with a large core, thin lines models with a small core.

the early formation of a thick compositional lithosphere, in contrast to the lower part of the mantle, which experiences less or no melting and retains its melt and will therefore be less viscous. The fraction of the water that is extracted from the mantle along with melt but not lost by outgassing is concentrated in the crust, which lowers the crustal viscosity. In principle, this change in crustal viscosity can destabilize the lithosphere, and some water can be transported back into the mantle by foundering of crust sufficiently thick that its base is in the stability field of eclogite. However, at the water concentrations of our models, such instability occurs only late in the evolution of model SC-LF, whereas, in general, the lithosphere only thickens with time and remains a stable stagnant lid.

The general style of all models is characterized by initially vigorous whole-mantle convection that weakens substantially within the first ~500 My, as can be seen in the animations of example models in the Electronic Supplement. Mean temperatures generally decline slowly but steadily after that initial stage, and mean viscosities rise as the mantle cools and loses water. Examples, shown in Fig. 2a, indicate that large-core models cool a bit more strongly so that their final mean mantle temperature is 50–80 K lower than that of their small-core counterparts, many of which go through a longer period of near-constant mean temperature. An increased water content also results in faster and stronger cooling, because the lower viscosity makes convective heat transport more efficient. The effect results in a ~40 K difference between the final mean temperatures of the 36 ppm and the 360 ppm models in the hL series but tends to be more pronounced in models with a low-viscosity lower layer. However, the evolution of mean temperature is not particularly sensitive to initial potential temperature. Mean viscosity and convective vigor depend most strongly on potential temperature and water content, as viscosity is most sensitive to these two factors. Their relative importance can be seen in Fig. 2b, which shows the mean viscosity of the upper layer, η_{UL}, as a function of age for some of the models. The more water-rich a model is, the lower is the mean viscosity, whereby the hotter SC models have slightly lower η_{UL} than the cooler LC models. As this viscosity partly controls the surface heat flux, water-rich models may be expected to have a higher heat flux (cf. Section 4.2). The extent of degassing, however, has no appreciable effect on dynamics, because in the dg models, where this parameter was varied, there was no crustal recycling; therefore, any water-bearing melts extracted from the mantle removed water from its convective system permanently, regardless of whether that water was outgassed or incorporated into the crust. Generally, convection slows monotonically with time, most strongly in the first few hundreds of millions of years, due to the substantial early dehydration of the uppermost mantle. After that initial stage, the effective Rayleigh number, defined as the Rayleigh number calculated from surface values divided by the mean viscosity, remains at a nearly constant level, decreasing further by no more than a factor of 1.5–2 until the present. The only exception to the monotonic trend appears in the LF models, in which Ra_{eff} reaches a local maximum at intermediate times as a consequence of stronger internal heating.

During the main stage of the planet's thermal evolution, convection becomes quite sluggish, and root-mean-square mantle flow velocities drop to values of 2 cm/y or less. At 4 Gy, convective vigor as parameterized by the effective Rayleigh number has decreased by at least half an order of magnitude compared with initial values. Two convective patterns dominate the processes in Mars' sublithospheric mantle: small instabilities descend from the outer thermal boundary layer into the deeper mantle, and plumes rise from the CMB. The small lithospheric instabilities mix the depleted melting zone back into the deeper mantle, sometimes to the effect of partly eroding it until this zone is incorporated into the stable thermal boundary layer. The number of plumes generally lies between 1 and 12 but often varies greatly with time, in some cases in a quasi-periodic way with apparent periods of several hundred million years. The only regular pattern in plume numbers appears to be that models with a very viscous

lower (and possibly basal) layer (hL and xL) tend to form a decreasing number of plumes as the models evolve, whereas in models with the reference viscosity setup, in which the viscosity of those deep layers is smaller than in the upper layer, the number remains strongly variable and shows no decrease. It is the type of radial variation of viscosity that is decisive for the reduction of the number of plumes, not the absolute viscosity, as is revealed by a comparison between the model pairs hL, hLA0.2, and hLA10, which do not show a systematic relation between mean viscosity and plume numbers. Whereas the plume count in hL models can drop to 2–4, the plumes are not stable, stationary structures. Nonetheless, in several models successions of plumes form within a limited area. The only marked exception is the xL model pair, especially model SC-xL, in which there is a quite clear evolution towards a stable pattern with two large plumes at approximately opposite locations in the mantle that occurs through mergers of 6–8 smaller initial plumes. In model LC-xL, a two-plume pattern is reached after 2.5 Gy, but occasionally one or two smaller additional transient plumes appear and are quickly dragged towards one of the two main plumes, whereas in model SC-xL a configuration with two stable plumes emerges shortly after 2 Gy and is not interrupted by transients thereafter. An animation of the latter model can be viewed in the Electronic Supplement.

Snapshots of the temperature, water concentration, and viscosity of models LC-hL and LC-180hL at a late stage (∼3.4–3.6 Gy) in their evolution are shown in Fig. 3 as examples of models with low to intermediate water concentrations that fit several observations reasonably well. The plots show that the wetter model has cooled more strongly and indicate that it features fewer plumes at that stage than the dryer model, but the viscosity is nonetheless lower in the wetter model. The mean water content does not fall far below the initial values in the deeper mantle as a consequence of refertilization by recrystallizing water-bearing melts. Especially in the wetter model, this zone has been larger in the early stages of evolution, but the depleted layer has subsequently been eroded by cold lithospheric downwellings as well as by the convection of the sublithospheric, subsolidus mantle.

The four groups of viscosity models for the lower layer of the mantle differ markedly in terms of dynamics. In the "reference" cases, the distribution of water gives rise to a substantial drop in viscosity at the top of the lower layer, whereas the eL and hL models show only a minor and smoother decrease and the xL models feature a marked increase. Apart from the existence of a basal layer, this viscosity structure and the initial bulk water content are the most important parameters controlling the thermal evolution of the mantle. The final laterally averaged profiles versus pressure and depth of temperature T, bulk water concentration C_w, viscosity η, and the absolute value of the vertical root-mean-square velocity are shown in Fig. 4 for several models in which these parameters are varied. The increasing vigor of convection in the more water-rich models leads to more efficient cooling of the mantle, at least of the upper layer; this effect is already visible a few hundred million years after the beginning. The low viscosity in the lower layer of models (L,S)C-ref, (L,S)C-180, and (L,S)C-360 generally entails relatively high flow velocities in most of the sublithospheric mantle, in spite of the low values of the thermal expansion coefficient and gravitational acceleration in the lower layer. Convection encompasses the entire sublithospheric mantle, i.e., there is no layered convection proper. Nonetheless, depth profiles of horizontal velocity (not shown in the figure) indicate that there are convective subsystems that are confined to the upper or the lower layer; this is especially true for the SC models. By contrast, the hL and xL counterparts of those models, which show a much smaller or no viscosity decrease in the lower layer (Fig. 4c), are characterized by very low vertical velocities in the lower layer independent of the water content, and the partial layering component is strongly reduced. In the models with a low-viscosity lower layer, partial layering of convective flow is established such that a fraction of upwelling material is diverted laterally. Hence the efficiency of heat removal from the deep mantle through the upper layer is diminished, so that the lower layer remains hotter by several tens of degrees in those models; especially in the SC cases, the lower layer may even heat up. If the core is small, the lower layer is underlain by a thin (pv + fp) layer that shows little interaction with the rest of the mantle, heats up, and acts as a basal heating source for the lower layer as well as a top heat source for the core that suppresses dynamo action. The hot lower layer would eventually evolve into a situation that is gravitationally unstable. In most of our models, the result is the formation of occasional small and rather weak plumes, although some models also produce one or two large transient jets in the last few hundred million years; a global overturn of the mantle is conceivable but does not happen within the lifetimes of our models.

3.3. Melting and crust formation

Melt production is highest in the first few hundred million years, when temperatures are still high, and drops to very low rates thereafter. Crustal thickness increases more steeply and reaches slightly higher values in water-rich models, especially in the LF pair, which is also more strongly internally heated. Nonetheless, with the exception of the LF pair the final thickness is almost reached after ∼1.5 Gy in LC models and after 2–2.5 Gy in SC models, and crustal growth continues at very low rates only in some localized areas thereafter. In particular, in the xL models the long-lived, quasi-stationary plumes cause the uninterrupted formation of a thick crust above them throughout almost the entire 4 Gy of evolution modeled. These areas tend to be larger in water-rich models, and more so in those with a high-viscosity lower layer, but the fraction of the surface area with more than 10 m/My growth generally lies below 15% in the second half of the models' duration. The greater effective Rayleigh number of models with initially high T_{pot} or high water content also means that more material is processed in the melting zones, so that such models produce more basalt in their lifetimes than cooler or low-water models. The effect of temperature on crustal productivity is stronger than the effect of water and is especially dominant in the strongly heated LF models; the increase in final crustal thickness with increasing water content is less than linear. As in RTS1, the SC models, which are productive over a longer time span, reach slightly higher final thickness values. As mentioned before, the crust does not generally grow to a thickness that allows the transformation of basalt to eclogite, so that crustal growth is a monotonic function of time; the only exceptions are models SC-LF and SC-xL. In model SC-LF maximum thicknesses exceed 200 km around 3 Gy, so that foundering of crustal roots results in thinning by several tens of kilometers. In model SC-xL, the crust above the two plumes begins to grow slowly into the stability field of eclogite after ∼2.2 Gy, but the growth rates are too low and the viscosity of the lithosphere too high for those roots to become unstable within the lifetime of the run; the eclogitic roots can be seen in the animation as dark blue patches at the 5 o'clock and 11 o'clock positions in the panel depicting the pyroxene and garnet assemblages ($\phi_{px/gt}$).

In the early stages of the models, the degree f of partial melting in the shallow mantle typically reaches a maximum value between 0.15 and 0.2 in the upper-mantle melting zones of most models; in the low-temperature pairs, it lies a bit below 0.15. Increasing water contents do not have a major impact on the maximum value of f, but they do depress the solidus, although the effect is not substantial at the relatively low water concentrations considered here. Melt generation in Mars was probably spread over a large depth range that reached into the stability field of ringwoodite and maj-

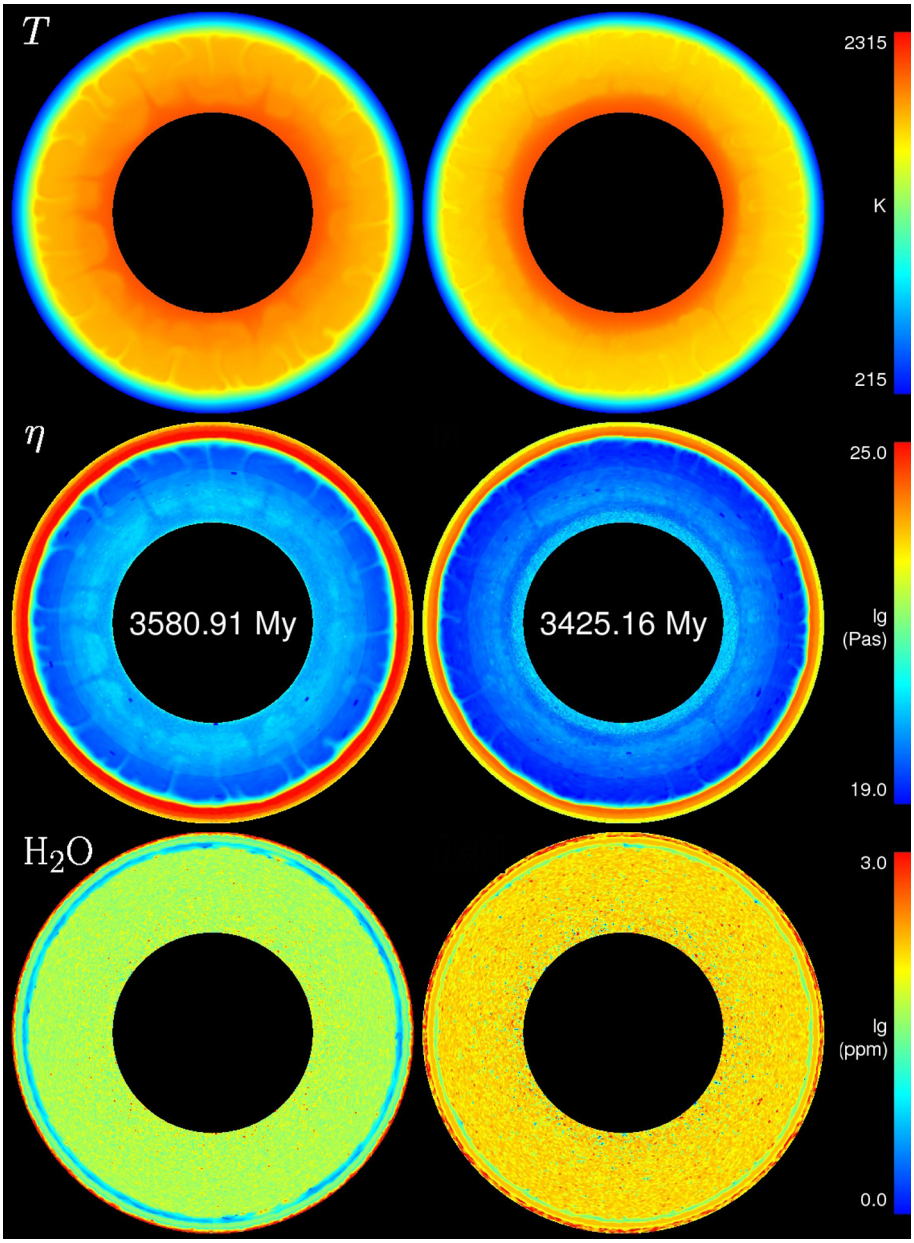

Fig. 3. Late-stage snapshots of temperature (top) and the decadic logarithm of viscosity (middle) and water concentration (bottom) for large-core models with a high-viscosity lower layer, an initial potential temperature of 1873 K, and radionuclide concentrations from Wänke and Dreibus (1994). The initial water content is 36 ppm in the model in the left column and 180 ppm in the model in the right column. The color bars of the viscosity and water concentration plots are clipped for improved display. See online version for color image. (For interpretation of the references to color in this figure legend, the reader is referred to the web version of this article.)

orite, as suggested on chemical grounds by Draper et al. (2003) and Shimoda et al. (2005). At the bottom of the mantle, the superheated core and later the preservation of high temperatures in the lower layer caused some melting in the deep mantle, but most of this melt remained trapped and in place because of the density crossover of melt and solid with increasing pressure or because a thick layer of solid material in the mid-mantle prevented its extraction.

3.4. Radionuclides and water

As a consequence of the limited extraction of melts and the apparent role of recrystallization and remixing, most of the radionuclides and water remain in the mantle, and enrichment of the crust in these components is generally minor compared with the initial bulk concentrations, although crustal concentrations can exceed those in the strongly depleted asthenospheric melting zone by one or two orders of magnitude, similar to the dry models of RTS1. The fraction tends to be slightly higher in models with a large core, but the absolute surface concentrations show no particular sensitivity to the size of the core. As one would expect, the surface and average crustal concentrations of water decrease with higher degassing fraction and increase with increasing water contents of the mantle source. They approach a final value as crust formation ceases, while radionuclide concentrations decrease according to the respective decay constants. The depth profiles in Fig. 4b show that the crustal water concentrations are not homogeneous but show some variation with depth, with the maximum reached in the lower crust in several cases. This shape reflects temporal variations of the water content of erupted material during model evolution. Specifically, if the erupted material is, on average, more water-rich at an early time, whereas later the mantle sources from

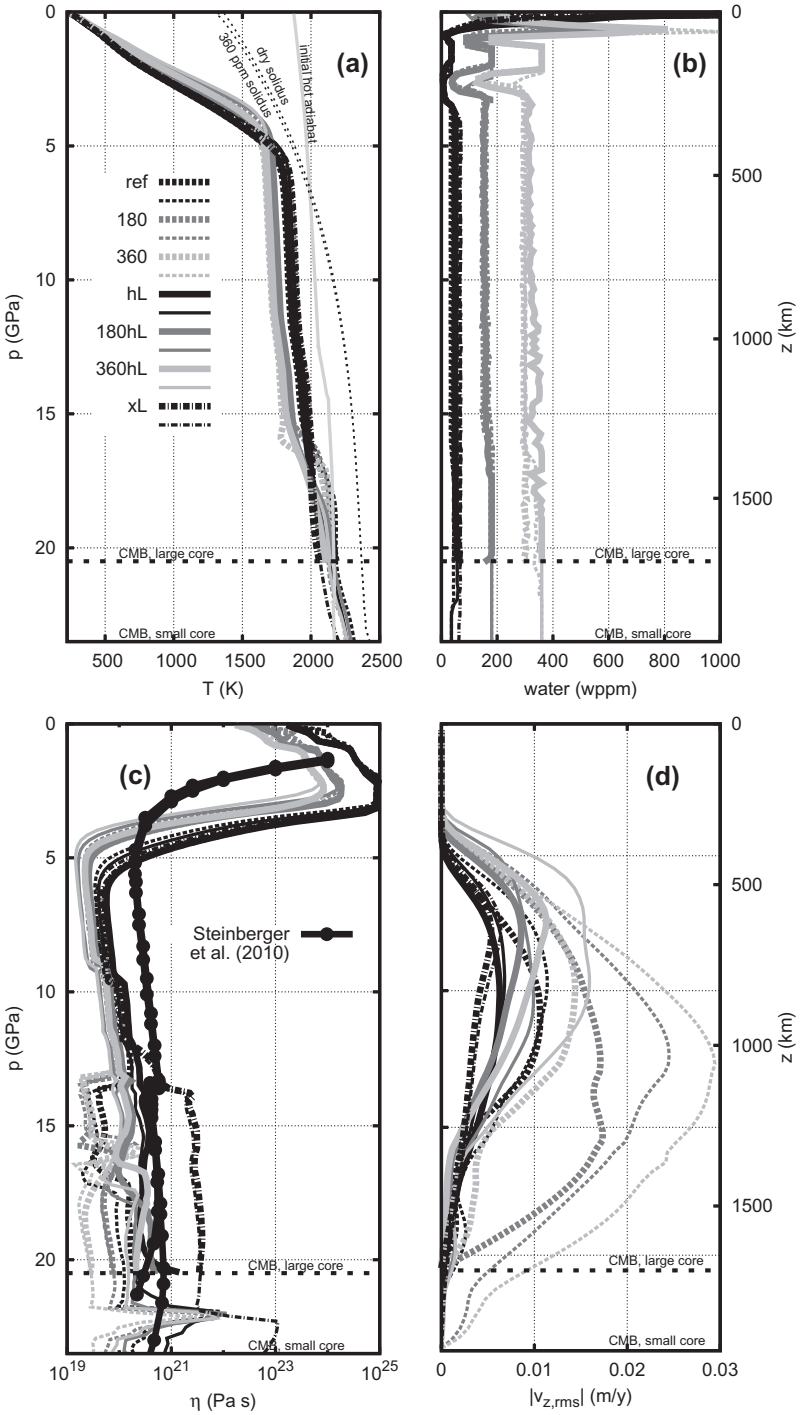

Fig. 4. Horizontally averaged profiles versus depth at 4 Gy for selected models: (a) temperature, solidus temperatures for 0 and 360 ppm bulk water, and example initial adiabat; (b) bulk water concentration; (c) viscosity; (d) absolute value of mean vertical velocity. Thick lines designate LC models, thin lines SC models. The viscosity plot also includes $\eta(z)$ models after Steinberger et al. (2010); note that absolute viscosities were not constrained in their study.

which the crustal material is derived become more depleted, then a deep crustal maximum is expected. As no crustal recycling takes place in almost all of the presented cases and mass transport within the crust is essentially vertical, the record of this evolution is preserved in the crust throughout martian history. Although we expect the particular shape of the depth profiles from our models to be controlled considerably by the initial conditions and also by the limited spatial resolution of the grid, and although the shape would be modified if a certain fraction of the melt extracted from the mantle were inserted into the deeper crust by intrusion instead of erupting at the surface, the general evolution of the planet makes it probable that the martian crust is less depleted at depth. Although our models do not allow predictions of the elastic and plastic response of the lithosphere, compositional heterogeneity of this type would influence the strength envelope of the lithosphere and should be considered in corresponding studies. Modeling of wrinkle ridges on Mars by Montési and Zuber (2003) supports the idea that the lower crust is ductile in regions with an old crust such as Solis Planum. In the deeper mantle, radionuclide and water concentrations show only minor changes with

time apart from those related to radioactive decay, so that radionuclides contribute to heating of the deep mantle for a long time, and the signature of water in the viscosity profiles does not undergo major changes. Because melting in the uppermost mantle occurs within the first billion years and becomes weak and ever more localized thereafter, a substantial part of the mantle probably contributes little to volcanism and likely preserves its original composition.

3.5. Mantle properties

Similar to the results given by RTS1, the relative proportions of the upper, lower, and basal layers are found to change in response to the thermal evolution of the mantle. At later stages in many models, the lower layer grows slightly at the expense of the other layers. However, especially in SC models with low water contents, the fraction of the upper layer remains almost constant for billions of years, whereas the lower and basal layer go through opposite volume changes as a consequence of intermediate heating of the deeper mantle.

Generally speaking, temperature and water content have the strongest influence on viscosity, as becomes obvious from comparison of the temperature, water content, and viscosity profiles in Fig. 4a–c. This sensitivity is also reflected in the effective Rayleigh number, which increases with either of these factors. Dehydration due to melting increases the viscosity substantially, especially in the water-rich models, and creates a compositional lithosphere, which merges with the thermal lithosphere as the mantle loses heat through the planetary surface. At that stage, the vertical variations of viscosity due to the effect of melting on water content are overwhelmed by the thermal diffusion profile in the upper mantle, but the influence of water content is still reflected in the thickness of the lithosphere, which is notably thinner in water-rich models. In this context it is worth noting that enforcing a general reduction of the viscosity by a factor 5 as we did in the hLA0.2 model pair has an effect very similar to raising the initial water concentration from 36 to 180 ppm on many characteristics of the model related to the vigor of convection, but some characteristics related to melt production and, obviously, chemical composition are noticeably distinct. This is expected from Eq. 2 given the finding that water concentrations in the deeper mantle did not vary greatly during the evolution of the models (cf. Section 3.4) and highlights that some "global" effects of water could be mimicked by simple multiplication with a constant factor, but that the effects of water that are more locally confined such as those related to melting would be missed with such simplifications.

4. Discussion

4.1. Dynamical and thermal evolution, and mantle properties

The models of this study sample a continuum of convective vigor, which increases with initial temperature and with the concentration of water in the mantle due to their effect on viscosity, melt production, and crust formation. The inclusion of water and the uncertainty about its effect on the viscosity of high-pressure forms of mantle minerals prompted us to consider different cases, one of which results in a local viscosity maximum at mid-mantle depths and a low-viscosity lower layer, and a set of other models (eL, hL, and xL) with higher viscosities in the lower layer and, except for xL, a generally more uniform viscosity throughout the sublithospheric mantle. The hL case is more similar to the dry-rheology models of RTS1 as far as the general shape of the viscosity–depth relation is concerned and can thus be seen as an extension of RTS1 in that the corresponding models follow a similar evolution, but at an accelerated pace due to the lower absolute viscosity.

We should emphasize that the viscosity depends on a variety of factors, and on some of them quite strongly, in a way that is non-unique in the sense that available observations for Mars do not have an accuracy and level of detail that would allow one to establish an unambiguous causal relationship between one of these factors and a given rise or drop in the viscosity. The important trade-off between temperature and water content has already been mentioned above: a softening of the material could be caused by an increase of either of them, or both. In RTS1 and this study, it is these two factors on which we focus in the first place, because previous numerical modeling studies as well as analyses of spacecraft data or meteorites have already provided some information that allows us to put bounds on them. By contrast, comparison of the hLA models with the hL, 180hL, and 360hL pairs (Section 3.5) points to at least one other potentially significant trade-off, namely between water concentrations or temperature and variations in the parameters A or b (grain size) in Eq. 2; the global change of η by a constant factor can be interpreted as representing the uncertainty in A, b, or b^3/A. The mineralogical composition of the martian mantle, although not completely uncontroversial, is considered to be peridotitic and hence dominated by olivine or its high-pressure forms in the most widely used chemical models, so that A is as well-defined as is E, V, or a, and the uncertainty about them depends on how well the assumption that the volumetrically dominant phase for which reasonably good experimental data are available – olivine – controls the rheological properties is fulfilled. The grain size, b, is a quite different problem, because it is not that well-constrained even for Earth. We can hence only rely on the rather scarce and indirect evidence as reported by Hirth and Kohlstedt (2003) that it is on the order of 1 cm but note that due to the dependence of η on its third power in the case of diffusion creep, even changes by a factor $\sim$2 would approximately correspond to the differences between the hL, hLA0.2, and hLA10 pairs.

Inferences about details of the viscosity structure of Mars are difficult to deduce from observations. Bills et al. (2005) have inferred a very low effective viscosity of 8.7×10^{14} Pa s from tidal interactions with Phobos for the martian interior, which they attribute in part to a low viscosity of the mantle. While their inference could support the case for a low-viscosity lower layer, it is important to note that their estimate is for a homogeneous Maxwell body, and it is difficult to identify the contribution of the mantle to this result. A low viscosity in the deep mantle is also at odds with the more detailed viscosity profiles derived by Steinberger et al. (2010) for the martian mantle, which show only a small decrease at the mid-mantle phase transitions. Absolute viscosities are not constrained in their model, but their profiles lie within an order of magnitude of those of our hL models in the sublithospheric mantle and have a similar shape, which is the case neither for our reference-viscosity models nor for the xL pair (Fig. 4c). Steinberger et al. (2010) also assumed a temperature step of 200 K across the CMB, which is almost certainly an overestimate and is probably the reason for the differences at the base of the mantle.

The Steinberger et al. (2010) viscosity profiles also indicate that the viscosity of the lithospheric mantle is very high, and this property is reproduced in our models as well, although the thickness of the lithosphere is markedly greater even in the more water-rich ones. A possible reason is that we followed the example of most previous convection studies and did not include dislocation creep in our rheological law, which might prevail in the pressure range in which the difference between Steinberger et al. (2010) and our models is largest (cf. Karato and Wu, 1993) and which might result in a lower effective viscosity there. The thickness of the lithosphere contributes to stabilizing the lid, but the combination of the thin-

ner Steinberger et al. (2010) lithosphere and the lack of evidence for crust/lithosphere recycling from geological mapping shows that even a somewhat thinner lithosphere should remain in the stagnant-lid regime that characterizes all of our models. Earlier models (Ruedas et al., 2009) not included here suggest that a much weaker lithosphere is required to produce a mobile, recycling lid. As the flow velocities are generally very low in the upper layer, especially at later stages of evolution, and as diffusion creep probably dominates much of the martian mantle including at least a part of the lithospheric mantle (Karato and Wu, 1993), we are confident that our rheological law does not oversimplify the rheology of the mantle to the point that it suppresses recycling of the lithosphere. Furthermore, the absence of eclogite in the deep crust and the progressive incorporation of depleted mantle into the lithosphere as the upper thermal boundary layer thickens also contribute to stabilizing the lithosphere by buoyancy.

Plumes with lifetimes of billions of years, such as those invoked to account for the long-lived magmatism at the Tharsis and Elysium volcanic provinces (e.g., Phillips et al., 2001), are not seen in any of the models except the xL pair. However, the different classes of lower-layer viscosity models follow different evolutionary paths with respect to plume formation. The reference viscosity models, whose mean mantle temperatures remain a bit higher, tend to develop many plumes during their lifetime and are therefore difficult to bring into agreement with the two-superplume hypothesis for the formation of Tharsis and Elysium. By contrast, the hL models produce fewer plumes at later stages, and although these are not long-lived, spatially stable structures either, there is a tendency, especially in the LC variant of these models, for plumes to remain within a certain region for extended periods rather than to emerge and move around markedly. The xL pair continues that trend and results in stable or almost stable patterns with two plumes, although the times when that happens may still be somewhat too late to match observations at Mars. When considering the number and stability of plume convection, it must be kept in mind that models in this study are two-dimensional and therefore lack the additional spatial degree of freedom of a three-dimensional spherical model, even though it has been shown that various diagnostics obtained with a spherical annulus grid as in our models agree better with their analogues from a fully spherical grid than those from a conventional cylindrical annulus (Hernlund and Tackley, 2008). Furthermore, two-dimensional models probably overestimate the time required for long-wavelength convection to become established, because it is difficult for two-dimensional plume sheets to 'move past' the downwelling sheets to merge into a large plume.

As was the case in RTS1, the models in this study do not result in degree-one convection, which has been suggested as a potential explanation for major features of Mars such as the crustal dichotomy and the existence of the Tharsis volcanic province. Zhong and Zuber (2001) presented a set of two-dimensional spherically axisymmetric models in which they imposed a depth-dependent viscosity structure with a weak asthenosphere and demonstrated that the presence of a viscosity contrast between the asthenosphere and the underlying deeper mantle of at least two orders of magnitude could produce a degree-one convection pattern. Roberts and Zhong (2006) showed that the viscosity contrast may be only approximately one order of magnitude in three-dimensional spherical models but confirmed that the contrast needed to be sharp to induce this mode. Our xL model pair confirms the tendency of a strong, sharp mid-mantle viscosity increase to foster low-degree convection with stable plumes, although the determination of the minimum contrast necessary to produce it must be left to three-dimensional spherical models. Nonetheless, the work of those authors suggests that a marked viscosity increase at the mid-mantle phase transitions would still be necessary, so we expect that the absence of a stable low-degree planform and the transient nature of individual plumes we infer from our reference-viscosity and hL series will persist in three dimensions. Furthermore, the differences in the dynamical evolution of LC-xL and SC-xL indicate that the presence of a basal pv + fp layer helps stabilize such a pattern, even though it does not seem to be a necessary condition. Although we cannot exclude the possibility that such a radial viscosity profile may have existed as a consequence of the overturn of a crystallizing magma ocean (e.g., Roberts and Zhong, 2006) in the earliest few hundred million years of martian history, a time period not included in our models, neither the experiment-based rheological law we use nor the viscosity profiles from Steinberger et al. (2010), which were validated with areoid measurements, lend support to the presence of a sufficiently strong viscosity contrast in more recent martian evolution. Nor did studies that considered a variety of observations in addition to the areoid (Kiefer et al., 1996; Sohl and Spohn, 1997; Defraigne et al., 2001) find rheological models with a marked steplike increase of the viscosity at mid-mantle depths to be successful. Hence, if degree-one convection did exist in the martian mantle and if a viscosity step beneath the asthenosphere is the only feature that can produce it within sufficiently short timespans, as suggested by Zhong and coworkers as well as our own models, then both must have been transient features of early Mars that may have been of a compositional nature and were obliterated by later convection. In that case it remains to be seen if stable superplumes generated by a degree-one or degree-two convection pattern can persist for billions of years even if the radial viscosity structure that had once brought them forth has vanished or if the concentration of volcanic activity at a few centers must be attributed to other causes. Alternatively, external causes have to be considered as triggers for a quick onset of degree-one convection. Mega-impacts in the earliest stage of martian evolution have been shown to be a possible cause for the crustal dichotomy (e.g., Marinova et al., 2008; Nimmo et al., 2008), and several studies have demonstrated that a large impact can trigger the formation of a superplume and extensive melt production (e.g., Reese et al., 2004; Golabek et al., 2011; Ghods and Arkani-Hamed, 2011).

Recent geomorphological analyses of volcanic edifices by Neukum et al. (2010) and Robbins et al. (2011) indicate that although volcanic activity was concentrated in a few distinct volcanic provinces during most of martian history, it was neither narrowly focussed within any single province nor steady. Both studies suggest that there were limited spatial shifts in volcanic activity within each province and that all volcanism was rather episodic. This picture is more easily reconciled with the episodic ascent of plumes within a larger region that we observe in the hL models than with the traditional notion of two long-lived superplumes, although we do not claim that our current models go beyond a fair qualitative agreement. The more water-rich of these models remain more productive in terms of crust building in the later stages of the planet's evolution, albeit at a very low level; if Mars is indeed volcanically active in localized areas to the present, or at least until the recent past, models with an elevated water content may explain this phenomenon more easily. Both models with a reference-viscosity and models with a high-viscosity lower layer can reproduce approximately potential temperatures between 1716 and 1803 K for Noachian mantle in the pressure range from 2.7 to 5 GPa that were suggested by Filiberto et al. (2010) and Filiberto and Dasgupta (2011) for the source region of basalts examined by the Mars rovers. Because temperatures do not fall as rapidly in the water-rich models of the hL subset as in those of the reference-viscosity series, however, the former models also tend to be volcanically a bit more productive in the late stage of martian history.

These considerations lead us to prefer the hL models over those with a low-viscosity lower layer and, as a corollary, lend support to

the finding by Chen et al. (1998) that the effect of water on the rheological properties of wadsleyite and ringwoodite is much smaller than on those of olivine. However, this conclusion hinges to some extent on the correctness of our assumption that martian mantle mineralogy is dominated by olivine and its high-pressure forms. If the martian mantle is instead dominated by pyroxenes and garnet, as suggested by Sanloup et al. (1999), we would expect the entire viscosity profile to be shifted towards even lower values, but the shape of the profile would probably not differ substantially from that of our hL models or that of Steinberger et al. (2010). The hLA0.2 pair gives an idea of the effects of such a shift on dynamics and observables and does not let it appear to be an appealing alternative. While this shift might offer an opportunity to reconcile to some extent our viscosity profiles with the low viscosities suggested by Bills et al. (2005), this problem is beyond the scope of this paper, and its investigation is impeded by the scarcity of rheological data for pyroxenes, garnet, and majorite under high pressure and temperature.

In agreement with the dry models of RTS1, we find that although the mineralogy and rheology establish a layered structure for the mantle, the mid-mantle phase boundaries are not a substantial obstacle to convective flow. Only the basal perovskite-rich layer in small-core models is somewhat separated and acts as a heat source for both mantle and core and as a thermal insulator between them. CMB temperatures in SC models vary even less than in RTS1 and preclude the onset of a core dynamo for at least the past 4 Gy. By contrast, LC models generally provide sufficient total core entropy to admit dynamo action during the first 0.5–1 Gy; at least for the hL models, there is a clear decrease of this time span with increasing water content and a slight decrease with decreasing mantle potential temperature, which suggests that models with elevated water concentrations and low potential temperature are most likely to agree with the duration of the actual martian core dynamo. Depending on the conditions at the CMB, the temporal evolution of entropy available for dynamo generation is not always a uniform decline; in models with a low-viscosity lower layer, and in particular in model LC-LF, there may occur one or more intermediate increases in entropy that may suffice to reactivate the dynamo at times up to ∼2.5 Gy. This may be interpreted as an additional argument against a low-viscosity lower layer, as there is no evidence for such events so late in martian history. The stronger decline in mantle temperatures in the LC models is also the reason why average mantle density increases in these models by 20–30 kg/m^3 over the past 4 Gy, whereas the rise in SC models lies between 10 and 20 kg/m^3; the density change is hence somewhat larger than in the dry models from RTS1, because those models cooled at a lower rate. We can also attempt an estimate of global contraction as in RTS1 and find again that the planetary radius would shrink by at least ∼10 km in LC models, but only by 3–5 km in SC models with 180 or 360 ppm water. The latter therefore agree better with the maximum radius decrease estimate of 3.8 km since the Early Noachian ($\gtrsim$ 4 Ga) derived by Nahm and Schultz (2011).

4.2. Surface heat flow and lithospheric thickness

The surface Nusselt number, i.e., the non-dimensionalized temperature gradient at the surface, is generally similar to those of RTS1 in these models. The initial water content of the models does not have a major effect. The heat flow q is closely related to the Nusselt number and can be derived directly from the temperature field. As in RTS1, we first calculated q from the temperature of the two uppermost grid rows and find similar values as in the dry models.

The ancient heat flow values inferred by McGovern et al. (2002) and Ruiz et al. (2006) from lithospheric flexure models matched to observed gravity and topography range from at least 30–40 mW/m^2 for areas of Noachian ($\gtrsim$ 3.5 Ga) age to $\lesssim$ 25 mW/m^2 for younger ($\lesssim$ 3 Ga) lithospheric loads; for the north polar regions, Ruiz et al. (2010) calculated a maximum current heat flow of 19 mW/m^2. If the planet cools inefficiently, as may be expected from a stagnant-lid system, the current heat flow may be as low as ∼10 mW/m^2 (Ruiz et al., 2011). To compare our results at least qualitatively with these values, which were calculated for a viscoelastic model with a non-Newtonian flow law and a thermal gradient averaged over the thickness of the mechanical lithosphere, we follow a procedure analogous to that in RTS1 and adopt a similar flow law for dry olivine and wet diabase and assume lithospheric stress levels of ∼10 MPa to determine the thickness of the mechanical lithosphere. Under these conditions, and considering the calculated crustal thicknesses in the early model stages, the properties of the mechanical lithosphere are probably controlled by water-bearing diabase, and the base of the mechanical lithosphere is estimated to lie somewhere between the 750- and the 1000-K isotherm, depending on water content. Water-rich models yield lithospheric thickness and heat flow values that lie close to the lower bounds from the flexure models for Noachian areas. For younger features, all of our models match well the estimates from the flexure model results. Fig. 5 shows curves for the mean lithospheric heat flux of the hL models; those for the low-viscosity models do not differ appreciably from their hL counterparts. As one should expect, the curves for the dry models of RTS1 are almost identical to those with an initial water content of 36 ppm, i.e., (L,S)C-hL, but increasing water contents raise q slightly, because the greater vigor of convection facilitated by the lower viscosity especially of the upper layer (cf. Fig. 2b) enhances heat transport towards the surface. The water-rich, high-^{40}K models (L,S)C-LF have even higher q but are still compatible with the independent data points. Models with a small core have slightly higher heat fluxes than models with a large core. In summary, although the influence of water leads to a larger variability in heat flux values compared with the bulk of the dry models of RTS1, the differences are too small to serve as a discriminant between "good" and "poor" models because of uncertainties in the independent data and the approximate nature of the comparison. Furthermore, there is a trade-off between core size and water content. The Heat Flow and Physical Properties Package (HP^3) experiment on the InSight mission (Spohn et al., 2012) should provide data that can be compared more easily with our model predictions, because the assumptions about the thickness of the elastic lithosphere could be omitted.

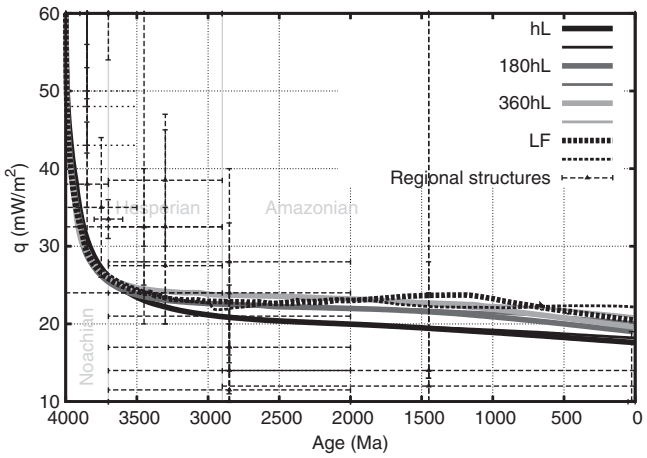

Fig. 5. Average surface heat flux as a function of time for the hL models with different water contents, and for the LF models.

The thickness of the elastic lithosphere we deduce in the process of deriving these mean lithospheric heat flows ranges from 170 to 240 km, with values for LC models up to 10 km larger than those of their SC counterparts. The lower values correspond to models with initial water contents of 180 ppm or more and the lowest ones to the LF pair, which features the additional softening contribution from stronger internal heating. The estimates of the thickness of the elastic lithosphere from which the aforementioned heat flux estimates from the literature were derived range from 150 to 300 km, whereas a similar calculation derived from limits to flexure under the north polar ice cap as measured by the Mars Reconnaissance Orbiter radar yields 300 km as a minimum value (Phillips et al., 2008). The parameterized thermal evolution study by Schumacher and Breuer (2006) also suggests values of 300–400 km. Steinberger et al. (2010) derived a lithospheric thickness of 240 km from an analysis of the gravity spectrum, which agrees quite well, especially with those of our models that have a large core and/or low initial water contents. Whereas the LF model pair also gives an acceptable match of heat flux and lithospheric thickness, the late-stage formation of eclogitic crustal roots and the beginning of crustal foundering in SC-LF indicates that these models should be dismissed, because Mars shows no signs of lithospheric disruption at least since the Middle Noachian (∼4 Ga, e.g., Taylor and McLennan, 2009). However, the appearance of these instabilities demonstrates that even a relatively small planet can experience a substantial change in convective style and possibly enter a new phase of geological activity at an advanced age under certain conditions.

4.3. Radionuclides and water

The redistribution of radionuclides and volatiles by melt production and extraction leads to an enrichment of these components in the crust, which can be compared with values derived from orbital remote sensing, rover/lander measurements, or martian meteorite analyses. The average radionuclide concentrations in our models show rather little variation among models. Table 3 lists average surface concentrations for ^{40}K and Th but not for total U, because K and Th are measured more frequently and with different methods, whereas U concentrations are often inferred and do not yield independent new information for our purposes. These mean concentrations are comparable with those of the reference models of RTS1, if slightly lower, and lie in a narrow range. They are thus also much lower than those derived from spacecraft and rover data but comparable to a subset of the meteorite data, which we deem representative of a larger crustal depth range and less affected by the near-surface processes discussed by Newsom et al. (2007) but probably biased toward recent ages and somewhat depleted mantle sources. By and large, our discussion from RTS1 applies to the radionuclide results of these models as well.

Water concentrations present a more complicated problem, because the role and extent of degassing are not well constrained, and inferences from chemical analyses show large uncertainties and ambiguities. In contrast to the radionuclides, the crustal mean water concentrations from our models span a range of more than an order of magnitude because of the different initial water concentrations and extents of degassing in the different models. In Table 3 we give both surface and whole-crust concentrations, because the combined effects of degassing and mixing of crustal material from extraction at different times has led to some intracrustal variability in the case of water. It is worth noting that in any given model, the variability of local melting conditions results in substantial compositional heterogeneity within both the crust and the mantle in spite of the homogeneous initial conditions, so that the compositional ranges of different models overlap. In general, total crustal mean concentrations increase with increasing water content in the source and decreasing degassing fraction. Furthermore, the hL models produce more water-rich crust than the models with a low-viscosity lower layer. We find that only a quarter or less of the trace components of the bulk silicate planet considered here fractionate into the crust, a fraction that is substantially less than the value of ∼50% given by McLennan (2001) or Kiefer (2003) and also somewhat less than the ∼40% estimate by Morschhauser et al. (2011). Ogawa and Yanagisawa (2012) found an even stronger fractionation into the crust but regarded their result as an overestimate. Our results are therefore in better agreement with the lower bound of 30% fractionation into the crust from Ruiz et al. (2006) or the estimate of Hauck and Phillips (2002) that only 5–10% of the water present in the mantle after initial degassing would be lost by volcanism at later times because of the inefficiency of degassing in one-plate planets. The full convection models by Plesa and Breuer (2011) also support the view that a one-plate planet such as Mars will release volatiles at a rather low rate.

Orbital gamma-ray and neutron spectrometry provide H abundances but do not reveal how the hydrogen is bound or where it originates (Boynton et al., 2008), so such methods yield only upper bounds for endogenic water. The tightest constraints on pre-eruptive water abundances in melts from the mantle are therefore probably those of Leshin (2000) on the basaltic shergottite QUE94201 and by Boctor et al. (2003) on melt inclusions in the dunitic Chassigny meteorite and indicate concentrations of a few thousand ppm (Table 4). Although abundances of 1.4–1.8% have been proposed on the basis of phase equilibria studies on the Shergotty meteorite, these high values may not be representative of the average mantle (e.g., Dann et al., 2001). By correcting for degassing, one can see that some of our models, especially those with higher initial water contents, can reach pre-eruptive melt concentrations of several hundreds or even more than 1000 ppm on average and with higher values locally. In general, our models yield somewhat lower water contents than these estimates, but they do fall into the lower part of the range of concentrations of the whole set of meteorite data. The values derived from rover or orbiter measurements are therefore at least one order of magnitude higher than both the meteorite concentrations and our results, but for the same reasons as with the radionuclides as well as the ambiguous interpretation of hydrogen concentrations derived from such measurements, the rover and spacecraft data may lead to overestimates of the mean crustal composition. On the other hand, the meteorites, whose ages do not generally exceed ∼1.4 Gy, may be more typical of late-stage melting of an already depleted mantle than of the bulk crust, and the extent of degassing they have experienced is difficult to quantify.

Hence, from a chemical perspective these results suggest that models with radionuclide contents from Wänke and Dreibus (1994) but initial water concentrations of at least ∼180 ppm and 50% degassing or more match observations best. These values are consistent with the estimate of $\leqslant$150 ppm for 3.9 Ga by Appendix Boctor et al. (2003, Appendix) from the ancient meteorite ALH84001. Higher concentrations in the lithospheric mantle of such models are also in agreement with the recent estimates of 140–250 ppm by McCubbin et al. (2010) for the source region of the 1.3-Gy-old Chassigny meteorite and of 73–290 ppm for the mantle source of the substantially younger shergottite meteorites (McCubbin et al., 2012). These estimates are sensitive to the efficiency of degassing, which depends on atmospheric pressure at the surface, among other factors. Whereas the pressure of the earliest atmosphere may have been as high as 10 MPa (Elkins-Tanton, 2008), the pressure range even for the early part of the time interval considered here was likely at least two orders of magnitude lower. From the style of volcanic eruptions on Mars, and for atmospheric pressures ranging at the end of the Hesperian (∼2.9 Ga, Taylor and McLennan, 2009) from 0.1 MPa to the current $<$ 1 kPa, Kusanagi and Matsui (2000) deduced a maximum concentration of 500–

Table 3
Approximate average surface concentrations of ^{40}K and Th (both in ppb by weight), and surface and total crust concentrations of water (in ppm by weight) at 4 Gy from models. CMB depths in the different model series are: LC, 1700 km; SC, 1950 km.

Model	Model feature	^{40}K	Th	H_2O	
				Surface	Total crust
LC-ref	Reference case	44	74	331	192
LC-dg0.1	10% degassing	45	75	665	346
LC-dg0.9	90% degassing	45	75	63	38
LC-180	180 ppm H_2O	45	72	107	267
LC-360	360 ppm H_2O	39	62	193	342
LC-LF	Tripled ^{40}K, 288 ppm H_2O	43	23	55	265
LC-Tpotl	$T_{pot} = 1773$ K	43	71	78	56
LC-v35	Surface porosity 35%	44	73	327	195
LC-eL	Elevated-η lower layer	46	76	676	284
LC-hL	High-η lower layer	49	81	1281	425
LC-180hL	180 ppm H_2O, high-η lower/basal layer	54	81	125	357
LC-360hL	360 ppm H_2O, high-η lower/basal layer	54	78	202	521
LC-TpotlhL	$T_{pot} = 1773$ K, high-η lower layer	46	77	244	85
LC-hLA0.2	As LC-hL, 5-fold decreased viscosity	53	74	23	78
LC-hLA10	As LC-hL, 10-fold increased viscosity	41	74	308	148
LC-xL	Very high-η lower/basal layer	50	84	1747	471
SC-ref	Reference case	43	71	305	150
SC-dg0.1	10% degassing	43	71	888	444
SC-dg0.9	90% degassing	43	72	81	42
SC-180	180 ppm H_2O	43	66	99	259
SC-360	360 ppm H_2O	42	67	199	423
SC-LF	Tripled ^{40}K, 288 ppm H_2O	87	47	228	408
SC-Tpotl	$T_{pot} = 1773$ K	42	69	153	68
SC-v35	Surface porosity 35%	43	70	306	216
SC-eL	Elevated-η lower layer	45	73	700	374
SC-hL	High-η lower/basal layer	49	77	2486	754
SC-180hL	180 ppm H_2O, high-η lower/basal layer	42	66	90	332
SC-360hL	360 ppm H_2O, high-η lower/basal layer	44	69	180	476
SC-TpotlhL	$T_{pot} = 1773$ K, high-η lower/basal layer	47	75	736	204
SC-hLA0.2	As SC-hL, 5-fold decreased viscosity	43	65	18	71
SC-hLA10	As SC-hL, 10-fold increased viscosity	42	75	742	281
SC-xL	Very high-η lower/basal layer	46	77	2966	715

2500 ppm for the martian mantle but pointed out that concentrations of one-tenth as great, i.e., 50–250 ppm, are more likely; the lower concentration corresponds to the higher atmospheric pressure. From an atmospheric density estimate of $\gtrsim 0.4$ kg/m^3 for Noachian or early Hesperian Mars (Manga et al., 2012), one can estimate the surface pressure at that time to be approximately 15–20 kPa; Cassata et al. (2012) derived a pressure of at most 40 kPa for 4.16 Ga from the ^{40}Ar/^{36}Ar ratio of the Noachian-age meteorite ALH 84001 and maximum pressures of 150 kPa for earlier times, which must be regarded as upper bounds, because they assume 100% degassing of crust-forming material. Under such conditions, the lower concentration estimates from Kusanagi and Matsui (2000) would also be consistent with 100–200 ppm water in the mantle sources of martian magmas. If inferred mantle water abundances point toward values of a few hundred ppm for the mantle source of meteorites of such different age as ALH84001, Chassigny, and the shergottite meteorites, which are considered no older than a few hundred million years on the basis of several isotope dating systems (Borg et al., 1997; Dreibus et al., 1996), this agreement can be seen as an argument in favor of a relatively low extent of secular degassing, as suggested by, e.g., Hauck and Phillips (2002), Ruiz et al. (2006), and our models. The low water concentration of Wänke and Dreibus (1994) of 36 ppm in the shergottite source would still be consistent with the higher reference concentrations of our more water-rich models if these meteorites represent young martian lavas and a substantially dehydrated recent upper-mantle source, whose water concentration would not exceed a few tens of ppm in the recent geological past.

We did not keep track of the degassed water directly during the runs. However, the fact that no crust is recycled into the mantle in nearly all models allows us to estimate the amount of water that is permanently lost from the deep planetary interior by degassing from the prescribed degassing factor, the concentration of water in the crust, and the thickness and density of the crust. The depth of a global ocean resulting from such a calculation ranges from 35 to ~200 m, i.e., a volume of 6 to $\sim 90 \times 10^6$ km^3, of which a part would escape into space; the only exceptions are the models with 10% degassing and some of those with low potential temperature, for which the global layer would be 12 m or less deep. A summary of these depths and volumes is given in Table 5 along with independent estimates.

Independent estimates of the depth or volume of such a global ocean equivalent have been made on the basis of several lines of geological and geophysical evidence and vary greatly. Clifford and Parker (2001, Fig. 11) arrived at a depth of $\sim$ 370 m for a surface porosity of 20% from an estimate of the amount of ice formed in the martian cryosphere in the course of time; we used this porosity value in most of our models. Although their maximum estimate for the global ocean layer is on the order of a few kilometers, the absence of evaporites and the presence of large rocks in regions where fine sediment would be expected if large bodies of water had existed is interpreted as an argument against such a large volume (Carr et al., 2010). Carr et al. (2003) considered deposits of the Vastitas Borealis formation throughout the northern plains in connection with the estimated transport capacity of Late Hesperian outflow channels and arrived at a global layer 156 m deep. By contrast, Boyce et al. (2005) analyzed the photogeologic evidence for sedimentary deposits of the same formation in impact craters and deduced that the northern lowland may have been covered by a body of water that corresponds to a global ocean almost three times as deep during the Late Hesperian/Early Amazonian (Table 5). The estimates derived from parameterized convection studies (Grott et al., 2011; Morschhauser et al., 2011) are up to one order of magnitude smaller, although the value of

Table 4
Approximate present-day average surface and total crust concentrations of ^{40}K, Th (both in ppb by weight), and water (in ppm by weight) inferred from observations.

	^{40}K	Th	H_2O
Meteorites (averages of bulk compositions)[a]			
Basaltic shergottites	19–330	42–730	236–603
NWA7034[b]	330	2635	$\lesssim$ 6000
	n.d.	n.d.	18000[c]
	n.d.	n.d.	2200–6400[d]
Olivine-phyric shergottites	16–180	11–409	3900
Lherzolitic shergottites[e]	18–117	27–150	813
Nakhlites (clinopyroxenites)[f]	105–495	150–850	1099–3404
Chassignites (dunites)	49–54	51–130	985
	n.d.	n.d.	1292–3170[g]
Orthopyroxenites	18	62	2145
Lander/rover measurements (Pathfinder, Spirit, Opportunity; averages)[a]			
Northern plains, rock[h]	68–913	126–1696	19200–74000
Northern plains, soils[e]	379–571	704–1070	6500
Spacecraft measurements (averages)[a]			
Northern plains	452	710	n.d.
Southern highlands	425	700	37000[i]
Various southern highland provinces	220–379[j]	360–620	n.d.
Various low-albedo provinces	97	166[k]	34000
Global crust (Phobos 2[l])	207–413	1900–3100	<45000
Global crust (Mars Odyssey GRS[m])	340–410	620–700	39000

[a] ^{40}K calculated from total K for a present-day fraction of 1.17×10^{-4} (Jaupart and Mareschal, 2003).
[b] Unclassified achondrite, partly similar to basaltic shergottites (Agee et al., 2013).
[c] Pre-eruptive, Shergotty (Dann et al., 2001).
[d] Apatite in shergottite QUE94201 (Leshin, 2000).
[e] Upper limit on Th (NWA6342) estimated from K/Th = 6660.
[f] Upper limit on K (NWA5790) estimated from K/Th = 6004.
[g] Melt inclusions in Chassigny (Boctor et al., 2003).
[h] Th inferred from K/Th = 4600 (TES surface type 2) (Taylor et al., 2008).
[i] Surface type 2 (Boynton et al., 2008).
[j] Baratoux et al. (2011), from K/Th = 5220 for ancient southern highlands (Taylor et al., 2006).
[k] Boynton et al. (2008), Poulet et al. (2009); with K/Th = 5000 for low-albedo data (TES surface type 1) from Mars Express, Observatoire pour la Minéralogie, l'Eau, les Glaces et l'Activité (OMEGA) (Taylor et al., 2006).
[l] Trombka et al. (1991), Surkov et al. (1994), probably biased toward southern highlands and Tharsis volcanic material.
[m] Taylor et al. (2006), Boynton et al. (2008), Taylor and McLennan (2009), Hahn and McLennan (2010).

14 m from the latter authors would be substantially larger if the degassing fraction were larger than their value of only 10%. Grott et al. (2011) found that the last significant volumes were emitted 3.5–2 Gy ago, an age that agrees well with the time at which crust formation ceases in our models (Fig. 6). If all of the present-day polar ice caps consisted of water ice, they would contain a water volume corresponding to a global ocean depth of 22–33 m (Zuber et al., 1998; Smith et al., 1999); to this, ice bound in subsurface deposits such as permafrost may add an amount considered minor by some workers (e.g., Christensen, 2006) but several times as large by others (e.g., Lasue et al., 2013). Lammer et al. (2003) estimated the amount of water lost to space over the past 3.5 Gy to correspond to a water layer of 12 m thickness, whereas other estimates put the loss for a comparable time span at 50–120 m (e.g., Krasnopolsky, 2000; Carr et al., 2003). Hence, the total amount of water degassed from the mantle would lie between 5 and 22×10^6 km^3 (a depth of 34–153 m), under the assumption that all such water is endogenic. If we consider on the basis of these estimates a global oceanic layer of a few tens to a few hundred meters depth as the most likely scenario, most of our models meet this constraint, and the more water-rich ones may meet it a bit better. Although one would tend to favor models with little degassing and discard those with extensive degassing on the basis of meteorite water contents, a substantial surface water body would require major water loss to the atmosphere. Given this trade-off, a degassing degree of 50% seems a fair compromise.

Information from isotopic measurements on martian meteorites indicates that their source regions were chemically isolated from each other within a few tens or at most a few hundreds of millions of years of martian formation, indicating that major parts of the mantle were not thoroughly mixed thereafter and that the martian mantle has ancient compositional heterogeneities (e.g., Chen and Wasserburg, 1986; Borg et al., 1997; Brandon et al., 2000). This result is also suggested by the large variability in meteorite elemental compositions. Our models, given their homogeneous starting condition, are unable to reproduce the full range of chemical variability, even though some compositional heterogeneity develops in all models as they evolve. This failing gives support for ancient heterogeneities, e.g., as the result of an early global mantle event predating the time window modeled in this paper (e.g., Elkins-Tanton et al., 2003). The existence of ancient mantle heterogeneities is also an argument in favor of lower water contents and a relatively high viscosity of the lower layer as in the hL models, because a mantle with such properties would convect less vigorously and hence be less well mixed (e.g., Schmalzl et al., 1996). Furthermore, the survival of those ancient heterogeneities suggests that they were large and did not contain substantial amounts of water, because their viscosity should have been one or two orders of magnitude larger than that of the surrounding mantle in order to remain identifiable after hundreds of millions or even billions of years (e.g., Spence et al., 1988; Manga, 1996). However, the volume of a garnet cumulate as proposed by Elkins-Tanton et al. (2003) would not be sufficient to produce a putative early high-viscosity lower layer as in the xL models and as proposed by Zhong and coworkers.

It has been speculated that the unusually high solubility of water in wadsleyite and ringwoodite has resulted in strongly elevated water concentrations in the transition zone of the terrestrial mantle and that the transport of water into the shallower mantle by convective upwelling leads to hydrous melting and the concomitant loss of incompatible trace components in a thin layer at the top of the transition zone as the water enters a mineral assemblage with a markedly lower storage capacity and a lower solidus temperature (Bercovici and Karato, 2003). Agee (2008) pointed out that dense melts could sit atop what we refer to as the lower layer for the same reason and produce the martian analogue of a seismic low-velocity layer near the terrestrial 410-km discontinuity. Our models were not designed to address this question, as dense deep melts remain trapped within their source and possibly refreeze there instead of segregating downward and accumulating in some deep layer. However, in our models even the highest water contents are far below saturation, and one of the simplifications in our model assumptions is a homogeneous initial distribution of water and radionuclides. Therefore, two conditions that are important for the formation of such a mid-mantle melt layer are not met. Furthermore, we note that the elevated iron content of the martian mantle is expected to increase the solubility of water in olivine, although the magnitude of this effect is not yet well constrained (Zhao et al., 2004; Withers et al., 2011). This and the presence of clinopyroxene, in which water has a larger solubility than in olivine (e.g., Hirth and Kohlstedt, 1996), should prevent the water content in mantle material crossing from the lower into the upper layer from reaching or exceeding the level of saturation.

4.4. Crustal thickness and magnetization

Mean crustal thicknesses lie between approximately 75 and 100 km for most models (Table 6). Only models with low potential temperature produce thinner crusts, whereas in the LF models the crust becomes much thicker as a consequence of the stronger

Table 5
Global ocean equivalent volume and depth estimates from models and inferred from observations. Loss to space is not included in the model estimates.

Model	Model feature	Volume (10^6 km^3)	Depth (m)
LC-ref	Reference case	6.2	43
LC-dg0.1	10% degassing	1.24	9
LC-dg0.9	90% degassing	11.1	77
LC-180	180 ppm H_2O	10	68
LC-360	360 ppm H_2O	13	90
LC-LF	tripled ^{40}K, 288 ppm H_2O	17.9	124
LC-Tpotl	$T_{pot} = 1773$ K	1.3	9
LC-v35	Surface porosity 35%	6.4	44
LC-eL	Elevated-η lower layer	9.4	65
LC-hL	High-η lower/basal layer	14.5	101
LC-180hL	180 ppm H_2O, high-η lower layer	13.7	95
LC-360hL	360 ppm H_2O, high-η lower layer	20.2	140
LC-TpotlhL	$T_{pot} = 1773$ K, high-η lower layer	2.1	15
LC-hLA0.2	As LC-hL, 5-fold decreased viscosity	3.2	22
LC-hLA10	As LC-hL, 10-fold increased viscosity	4	28
LC-xL	Very high-η lower/basal layer	16.3	113
SC-ref	Reference case	5	35
SC-dg0.1	10% degassing	1.7	12
SC-dg0.9	90% degassing	13	90
SC-180	180 ppm H_2O	10.8	75
SC-360	360 ppm H_2O	16.7	115
SC-LF	Tripled ^{40}K, 288 ppm H_2O	22.5	156
SC-Tpotl	$T_{pot} = 1773$ K	1.75	12
SC-v35	Surface porosity 35%	7.6	52
SC-eL	Elevated-η lower layer	13	90
SC-hL	High-η lower/basal layer	28.2	195
SC-180hL	180 ppm H_2O, high-η lower/basal layer	14.1	98
SC-360hL	360 ppm H_2O, high-η lower/basal layer	19.5	135
SC-TpotlhL	$T_{pot} = 1773$ K, high-η lower/basal layer	5.7	40
SC-hLA0.2	As SC-hL, 5-fold decreased viscosity	3	21
SC-hLA10	As SC-hL, 10-fold increased viscosity	8	56
SC-xL	Very high-η lower/basal layer	26.6	184
Other studies			
Boyce et al. (2005), Vastitas Borealis crater sediments		60	430
Carr et al. (2003), Vastitas Borealis sediments, outflow channels		23	156
Clifford and Parker (2001) fig.11 20% surface porosity, cryosphere ice		~53	~370
Clifford and Parker (2001) maximum, ice in cryosphere		159–405	1100–2800
Grott et al. (2011), thermochemical evolution model		2.5–8.8	17–61
Morschhauser et al. (2011), parameterized evolution model		2	14
Krasnopolsky (2000), loss to space		9.4–17.3	65–120
Lammer et al. (2003), loss to space since 3.5 Ga		>1.7	>12
Lasue et al. (2013), episodically from 0.2 to 4.5 Ga		23–144	160–1000
Lasue et al. (2013), modern polar deposits+cryosphere		11.5–34.5	80–240
Zuber et al. (1998), Smith et al. (1999), polar ice caps		3.2–4.7	22–33

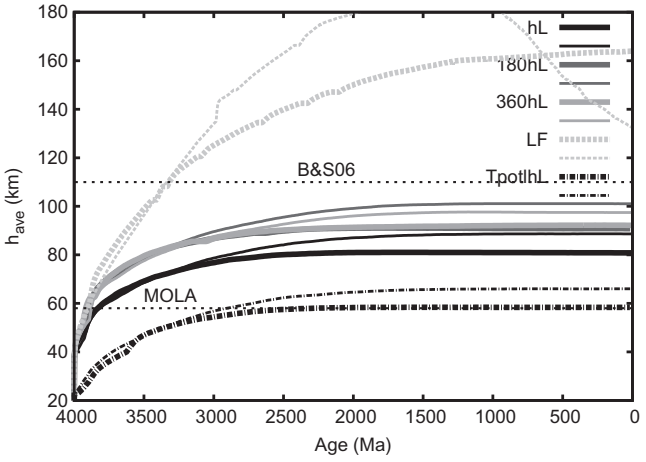

Fig. 6. Average crustal thickness as a function of time for the hL models and the LF pair. Also shown are the lower bound on the mean crustal thickness of the southern highlands inferred from altimetry and gravity measured by Mars Global Surveyor (MOLA, Neumann et al., 2004) and the upper bound from Breuer and Spohn (2006), labeled B&S06.

internal heating. An increase in mantle water content from 36 to 180 ppm has the effect of raising crustal thickness by ~10–20 km, but beyond that concentration there is no appreciable further increase. The low-water models (L,S)C-hL, which are most closely comparable with the reference models from RTS1, yield very similar crustal thicknesses, as they should. Whereas SC or hL models tend to produce thicker crusts than LC or reference-viscosity models, respectively, these effects are on the order of at most a few kilometers. As in RTS1, crustal growth is monotonic (except for model SC-LF), but the final thickness is approached more quickly (Fig. 6). The most important reason for this difference is the more vigorous convection facilitated by the lower viscosity of the mantle, by which the mantle, and especially the crust-producing upper mantle, is cooled more efficiently. Furthermore, dehydration and concomitant stiffening, which are absent in RTS1, will help to slow down convection and thereby reduce the rate at which fresh mantle material is processed in the melting zone. Our growth curves compare well with some of those from Schumacher and Breuer (2006) and Ogawa and Yanagisawa (2012) with respect to the time at which the final thickness is reached, although the latter authors start with a thicker initial crust. Nonetheless, most of our models might tend to overestimate the duration of crustal growth, which according to crater size–frequency

statistics had declined strongly by 3.7–3.5 Ga (e.g., Werner, 2009), unless crustal formation had shifted towards a more strongly intrusive mode that cannot be detected easily from orbiting spacecraft.

Independent estimates of crustal thickness range from 30 to 110 km (Table 6), whereby the most probable value is expected to lie between 50 and 100 km. It is therefore not possible to identify a favorite model on the basis of crustal thickness. The only firm conclusion is that the LF models can be discarded. The trade-off between potential temperature and water content indicates that if T_{pot} is a bit lower than 1873 K, elevated water contents can compensate for the reduction in crustal thickness to some extent. Furthermore, a much higher water content than 360 ppm would shift the basalt–eclogite transition to shallower depths (e.g., Litasov and Ohtani, 2007) and thereby induce crustal instability at some point, but there is no evidence from spacecraft imaging that such instability ever occurred on Mars.

Table 6
Crustal thickness at 4 Gy from models and inferred from observations.

Model	Model feature	$h_{c,ave}$	$h_{c,min}$
LC-ref	Reference case	77	62
LC-dg0.1	10% degassing	76	62
LC-dg0.9	90% degassing	77	60
LC-180	180 ppm H_2O	88	80
LC-360	360 ppm H_2O	90	80
LC-LF	Tripled ^{40}K, 288 ppm H_2O	164	100
LC-Tpotl	$T_{pot} = 1773$ K	56	41
LC-v35	Surface porosity 35%	78	62
LC-eL	Elevated-η lower layer	78	62
LC-hL	High-η lower/basal layer	81	67
LC-180hL	180 ppm H_2O, high-η lower layer	91	80
LC-360hL	360 ppm H_2O, high-η lower layer	92	79
LC-TpotlhL	$T_{pot} = 1773$ K, high-η lower layer	58	42
LC-hLA0.2	As LC-hL, 5-fold decreased viscosity	98	89
LC-hLA10	As LC-hL, 10-fold increased viscosity	63	48
LC-xL	Very high-η lower/basal layer	82	62
SC-ref	Reference case	79	59
SC-dg0.1	10% degassing	82	67
SC-dg0.9	90% degassing	82	68
SC-180	180 ppm H_2O	99	91
SC-360	360 ppm H_2O	94	86
SC-LF	Tripled ^{40}K, 288 ppm H_2O	132	52
SC-Tpotl	$T_{pot} = 1773$ K	60	41
SC-v35	Surface porosity 35%	83	69
SC-eL	Elevated-η lower layer	83	68
SC-hL	High-η lower/basal layer	89	71
SC-180hL	180 ppm H_2O, high-η lower/basal layer	101	91
SC-360hL	360 ppm H_2O, high-η lower/basal layer	97	84
SC-TpotlhL	$T_{pot} = 1773$ K, high-η lower/basal layer	66	43
SC-hLA0.2	as SC-hL, 5-fold decreased viscosity	102	91
SC-hLA10	as SC-hL, 10-fold increased viscosity	67	52
SC-xL	Very high-η lower/basal layer	88	64
Other studies			
Breuer and Spohn (2006)	standard model	110	
Cheung and King (2011),	southern highlands	~90–100	
Hauck and Phillips (2002),	nominal model	62	
Konopliv et al. (2006)		72	
Morschhauser et al. (2011),	preferred model	59	
Neumann et al. (2004),	global	>45	<15
Neumann et al. (2004),	southern highlands	58	
Nimmo and Stevenson (2001)		30–100	
Ogawa and Yanagisawa (2012)	reference model	~80	
Ruiz et al. (2008)		45–65	
Schumacher and Breuer (2006)		67–102	
Turcotte et al. (2002)		90	
Wieczorek and Zuber (2004)		50	38

The temperature distributions computed in the models allow the calculation of the depth to the Curie temperature for magnetic minerals. As the mantle cools, hematite and magnetite would reach their Curie temperature at greater depth, with such depths consistently ending up near or greater than the base of the crust at 4 Gy. Pyrrhotite usually reaches its Curie temperature of only 593 K near the base of the crust, although in some SC models with higher water contents a part of the lowermost crust may be temporarily hotter. In the LF models, the crust grows to a thickness at which its lowermost tens of kilometers heat beyond the Curie temperatures of all magnetic carrier minerals. However, unless crust that was once at much shallower levels becomes deeply buried by volcanic deposits, this heating should have little effect on the magnetic signature of the crust, because except for pyrrhotite in model LC-LF the critical thickness is reached at times when the core dynamo is about to cease or has already shut down. The more intense internal heating in the LF pair causes a steeper temperature gradient in the lithosphere so that in these models the Curie temperature and the brittle–ductile transition are reached at shallower depth than in the other models (Fig. 7).

As with the dry models of RTS1, our conclusion regarding the depth to the Curie temperature is that the lower values of 35–54 km (Nimmo and Gilmore, 2001; Ruiz et al., 2006; Voorhies, 2008; Ravat, 2011) are in better agreement with models having an initial potential temperature of 1873 K. The cooler models may have too thin a crust during the earliest era when the dynamo was active, although a recent study by Lewis and Simons (2012) found a mean magnetized shell thickness of only 26 km. The thicker magnetized crust suggested by Arkani-Hamed (2005) could at best be explained with model LC-LF, because only in this model does the crust grow to a thickness of more than 85 km during the period of dynamo operation, which lasts longer in this model than in others.

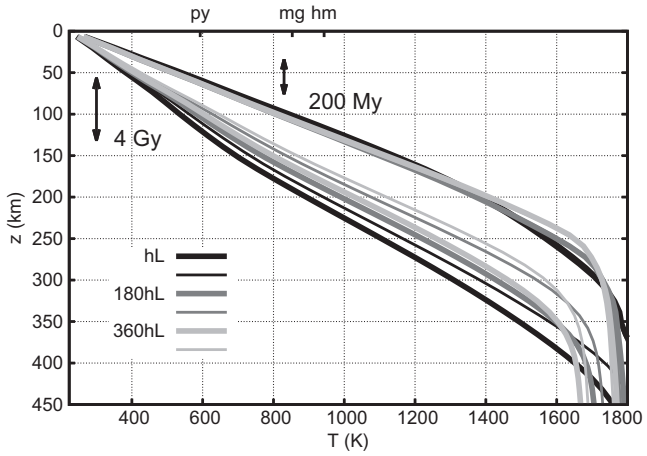

Fig. 7. Temperature profiles in the uppermost mantle for selected hL models at 200 My and at 4 Gy, respectively. The double-headed arrows indicate the range of crustal thicknesses of all models at the same times. The Curie temperatures for hematite (hm), magnetite (mg), and pyrrhotite (py) are also marked. In the set of 200 My profiles, the curves for models with large and small core are still very similar and thus not visible as separate lines here.

4.5. Areoid and moment of inertia

The computation of the full areoid requires a three-dimensional model, whereas models in a (two-dimensional) spherical annulus such as ours can reproduce only some general characteristics, because the continuation of the modeled structures into the third dimension is not defined uniquely. Such structures are expected to have the shape of a sheet that follows the curvature of the sphere in the vicinity of the model plane, but whether they depart from that shape at greater distances or not is unconstrained (Hernlund and Tackley, 2008), so the calculated areoid profile will not correspond precisely to that of an actual cross-section through a fully three-dimensional spherical model but should approximate it better than that of a conventional cylindrical cross-section. Because of these restrictions, we limit ourselves to a qualitative comparison of extremal values and the general shape of the spectrum with observations.

The spectra of the reference gravitational equipotential surfaces, or areoids, of the models at 4 Gy share a peak at degree 2 with the typical RTS1 models in many cases, but most models display additional large peaks at higher orders or do not decay with increasing harmonic degree as strongly as would be expected from satellite-derived spectra. In particular, models with a low-viscosity lower layer and initial water contents of 180 ppm or more have large degree-3 contributions, which in some cases are even stronger than the degree-2 term. The only models that feature a large maximum at degree 2 and then fall off quickly are LC-dg0.1, LC-Tpotl, SC-360hL and, because of their stable superplumes, the xL pair; the xL pair shows a particularly strong decrease for degrees $\gtrsim 8$. Fig. 8 shows the power spectral density of the areoid up to harmonic degree 20. Judging the modeled areoids by the extrema of the MGGM08A isostatic areoid of −332 and 639 m (Marty et al., 2009), all of the model areoids, especially the LF and the xL pair, match observations poorly in terms of extremal values, although the three aforementioned models that compare favorably with satellite-derived spectra at least come reasonably close (to within less than 100 m) to the observed minimum. The dynamic topography at 4 Gy seldom exceeds ±1 km.

The moment of inertia (MoI) can be estimated from laterally averaged radial density profiles and the formula for a radially symmetric sphere, as described in RTS1; the geometric properties of the spherical annulus permit a direct calculation of the MoI without the rescaling that would be necessary in other 2D grids. Present-day normalized moments of inertia in our models lie mostly between 0.3653 and 0.3659 (LC) and between 0.3626 and 0.3634 (SC), respectively (Table 7), whereas the best estimate for the mean moment of inertia of Mars lies between 0.36432 and 0.36538 (Konopliv et al., 2011), taking into account a reduction for the effect of Tharsis. The LC models, especially those with higher water contents and LC-LF, thus come quite close to the target values, whereas the SC models give too small MoIs, except for the two cases with low potential temperature and water content, which have an MoI of 0.3649. Correcting the observed MoI for the effect of a spherical cap that compensates for the crustal dichotomy as we did in RTS1 does not change the outcome markedly. There is thus a trade-off between potential temperature and core size in the effect on the MoI.

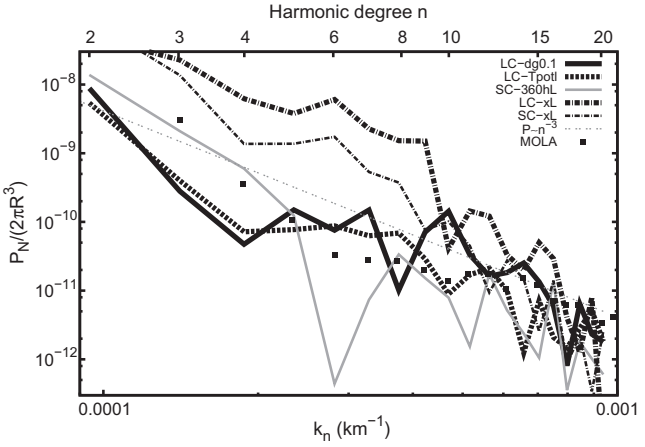

Fig. 8. Normalized power spectral density of the areoid P_N as a function of wavenumber $k_n = n/(2\pi R)$ and harmonic degree n for the three best models and the xL pair up to $n = 20$ at 4 Gy; also plotted for comparison are the coefficients from Mars Global Surveyor observations (MOLA) and the relation $P_N \sim 1/k_n^3$, known as Kaula's law (Turcotte et al., 2002).

Table 7
Normalized moment of inertia at 4 Gy.

Model	Model feature	MoI
LC-ref	Reference case	0.3658
LC-dg0.1	10% degassing	0.3658
LC-dg0.9	90% degassing	0.3658
LC-180	180 ppm H_2O	0.3655
LC-360	360 ppm H_2O	0.3655
LC-LF	Tripled ^{40}K, 288 ppm H_2O	0.3639
LC-Tpotl	$T_{pot} = 1773$ K	0.3676
LC-v35	Surface porosity 35%	0.3653
LC-eL	Elevated-η lower layer	0.3659
LC-hL	High-η lower/basal layer	0.3659
LC-180hL	180 ppm H_2O, high-η lower layer	0.3655
LC-360hL	360 ppm H_2O, high-η lower layer	0.3653
LC-TpotlhL	$T_{pot} = 1773$ K, high-η lower layer	0.3676
LC-hLA0.2	As LC-hL, 5-fold decreased viscosity	0.3651
LC-hLA10	As LC-hL, 10-fold increased viscosity	0.3666
LC-xL	Very high-η lower/basal layer	0.3659
SC-ref	Reference case	0.3634
SC-dg0.1	10% degassing	0.3633
SC-dg0.9	90% degassing	0.3633
SC-180	180 ppm H_2O	0.3626
SC-360	360 ppm H_2O	0.3628
SC-LF	Tripled ^{40}K, 288 ppm H_2O	0.3624
SC-Tpotl	$T_{pot} = 1773$ K	0.3649
SC-v35	Surface porosity 35%	0.3628
SC-eL	Elevated-η lower layer	0.3634
SC-hL	High-η lower/basal layer	0.3634
SC-180hL	180 ppm H_2O, high-η lower/basal layer	0.3627
SC-360hL	360 ppm H_2O, high-η lower/basal layer	0.3626
SC-TpotlhL	$T_{pot} = 1773$ K, high-η lower/basal layer	0.3649
SC-hLA0.2	As SC-hL, 5-fold decreased viscosity	0.3627
SC-hLA10	As SC-hL, 10-fold increased viscosity	0.3642
SC-xL	Very high-η lower/basal layer	0.3635
Other studies (mean moment of inertia)		
Konopliv et al. (2011), with Tharsis correction, lower bound		0.36432
Konopliv et al. (2011), with Tharsis correction, upper bound		0.36538

5. Conclusions

We have extended the simulations from Ruedas et al. (2013) of the thermal and compositional evolution of the martian mantle over the past 4 Gy in combined mineralogical and dynamical convection models to include the effects of water on melting and rheology. From the results, we also derived predictions for several quantities that are observed or inferred from observations. Comparison of our results with those independent findings shows that a subset of the models of this study matches some, but not all, of these quantities fairly well, the most important exception being the areoid. Nonetheless, some conclusions regarding the state of Mars's interior and its geophysical and geochemical properties may be drawn from our modeling.

The mantle properties that have the strongest influence on the dynamical behavior of the mantle are the presence or absence of a basal pv + fp layer and the viscosity. The latter is mostly controlled by the temperature and the water content. As a consequence, there is an important trade-off between these two variables: a lower viscosity can be caused by a higher temperature or a higher water content, or both. Furthermore, both also have a similar effect on the depth extent of melting and hence on the volume of crust produced. By improving the constraints on the water content of the mantle through geochemical observations and on the thickness of the crust, one can therefore deduce bounds on the temperatures in Mars using dynamical models, but any such attempt will still be affected by the uncertainty in other significant factors such as grain size. Models with low water concentration convect more sluggishly and cool less efficiently than models with higher water contents. If the lower layer of the mantle shows a strong rheological sensitivity to water content and has a low viscosity, its thermal evolution will diverge somewhat from that of the upper layer, which will cool more strongly. If the rheological effect of water on the lower layer is minor, the viscosity–depth relation will be more uniform, as will the thermal evolution of the mantle. The style of plume formation as well as the comparison with the viscosity profiles from Steinberger et al. (2010) favor a martian mantle whose lower part has a relatively high viscosity compared with our reference models and their water-rich variants, although a pronounced increase in viscosity in the lower layer as in the xL pair is neither supported by independent studies nor especially preferable with respect to criteria other than the stability of a low-degree convection planform. While our models tend to support the case for a rather weak effect of water on the viscosity of wadsleyite and ringwoodite, the profound impact of lower-layer rheology on the dynamics of Mars highlight that better experimental constraints on this property are needed.

With respect to some of the tighter and more important independent constraints, in particular the existence of a core dynamo and the moment of inertia, large-core models give better results than small-core models. On the other hand, many other observables are rather insensitive to core size, and a few, such as global contraction, rather favor small-core models; however, contraction is probably not as well constrained as other observables. The most important factor causing the differences between large-core and small-core models is the presence of the basal pv + fp layer, but its effect does not necessarily produce an unambiguous signature in currently accessible observables, with the possible exception of the viability of a dynamo.

In general, the more successful models initially have the radionuclide concentrations from Wänke and Dreibus (1994) as homogeneous initial abundances, but the preferred initial mantle water concentrations lie rather between those of Wänke and Dreibus (1994) and at least ∼180 ppm. Substantially higher water concentrations than 360 ppm or stronger internal heating than provided by the preferred radionuclide concentrations would result in lithospheric instabilities for which evidence is lacking. We suggest that the low water concentrations inferred by Wänke and Dreibus (1994) are more representative of the dehydrated younger upper mantle of Mars and have evolved toward that level from more water-rich conditions by dehydration during melting and formation of the crust. Although several of our models within the preferred range of compositional parameters reproduce subsets of crustal compositions inferred from martian meteorites fairly well and produce a certain degree of chemical heterogeneity as a consequence of melting and dynamical mixing, none reproduces the entire spectrum of compositions. This result supports the hypothesis that the martian mantle has ancient and long-lived heterogeneities and did not convect with sufficient vigor in the past 4 Gy to destroy them. All of the models that are at least marginally successful agree in that melt production and concomitant volcanism and formation of new crust have decreased strongly before the beginning of the Amazonian and that later production of crust was confined to small regions and volumetrically insignificant. Late volcanic activity is more widespread in models with a higher water content and with a higher viscosity of the lower layer. On the other hand, the compositional heterogeneity observed in martian samples is an argument against very high water contents that would entail more vigorous convection.

For various observables from the literature that can be compared with our results, e.g., the thickness of the crust or the lithospheric heat flux, good agreement can be found with a large subset of our models. This agreement is partly due to the large uncertainties in observations, but also a consequence of the dependence of such observables on many variables and the existence of certain trade-offs, e.g., between potential temperature and water content, with respect to them. Reduction of observational errors and the acquisition of new, additional observables, especially seismological data, which would allow much tighter constraints for instance on crustal thickness and core size, are necessary in order to narrow the range of admissible models. All three experiments on the InSight mission (i.e., seismometer, heat flow probe, and the geodetic package) are expected to facilitate major progress on these issues and in particular to settle the question about the size of the core. The seismological data it will deliver should also give more precise information about the thickness of the crust, and it may yield some information about the depth extent of melting and about attenuation in the mantle, both of which may help narrowing the range of admissible temperatures and water concentrations.

In summary, we cannot identify one single preferred model but can state that models with a large core and a high-viscosity (hL) lower layer give generally best results. The most probable initial radionuclide concentrations are expected to be close to those from Wänke and Dreibus (1994), but the water contents lie approximately between 100 and 200 ppm. 50% degassing is a plausible estimate for degassing of crust-forming material, whereby the fraction of mantle water that is lost by degassing is minor.

As in RTS1, it has not been possible to produce a convection pattern of one or two long-lived whole-mantle superplumes within the timeframe defined by martian geological history, except in the xL models, which require a radial viscosity model that is in conflict with other constraints. If such superplumes have indeed existed on Mars, they are therefore probably the result of heterogeneities in the thermal and compositional initial or boundary conditions, as has been suggested by previous workers. On the other hand, there is also the possibility that a succession of less long-lived plumes originating from within a limited region of the CMB has produced episodic volcanism, for which recent surface geological evidence provides some indication. Such a scenario would be easier to reconcile with the general character of convection in our models.

Acknowledgments

We thank an anonymous referee for thoughtful comments and Scott King for proposing a detailed discussion of models with a very high lower-layer viscosity. We appreciate helpful discussions with, and advice from, Lars Borg, Richard Carlson, Yingwei Fei, Konstantin Litasov, Francis McCubbin, Michelle Minitti, Ana-Catalina Plesa, and Jessica Warren. Francis McCubbin, Bernhard Steinberger, and their respective coauthors kindly shared preprints of their papers. The research reported in this paper was mostly supported by the NASA Planetary Geology and Geophysics Program through grants NNG04GI64G and NNX07AP50G. Resources supporting this work were provided by the NASA High-End Computing (HEC) Program through the NASA Center for Climate Simulation

(NCCS) at Goddard Space Flight Center, awards SMD-09-1310 and SMD-10-1816.

Appendix A. Loss of water (hydrogen) to the core

Shibazaki et al. (2009) carried out hydrogen partitioning experiments between ringwoodite, the major phase of the lowermost martian mantle in the case of a large core, and liquid iron and found a mass partitioning coefficient $D^{\mathrm{H}}_{\mathrm{Fe/rw}} = C^{\mathrm{H}}_{\mathrm{Fe}}/C^{\mathrm{H}}_{\mathrm{rw}}$ of ~9 (molar partitioning coefficient of 27.5) at pressures corresponding to the CMB and a temperature of 1273 K. On the basis of this result they suggested that almost all of the water transported to the CMB by putative ancient subduction would be absorbed by the core. This suggestion implies that some other parts of the mantle not involved in such subduction could also be dehydrated if they are brought to the CMB by convection. In this appendix we assess with a simple diffusion model the importance of the core as a water sink. For simplicity, we treat the core and the mantle as semi-infinite with respect to the transport of water, and we use the analytical solution for diffusion between two half-spaces. We further assume that near the CMB convective currents in both the mantle and the core are parallel to the boundary and that there is no lateral variation in concentration. Considering only diffusion, the transport of water can be described by the diffusion equation:

$$\frac{\partial C}{\partial t} = \kappa_{\mathrm{H}} \frac{\partial^2 C}{\partial x^2}. \tag{A.1}$$

The boundary condition at the CMB ($x = 0$) is defined by the partitioning coefficient between the two phases as $D^{\mathrm{H}}_{\mathrm{Fe/rw}} = C_{\mathrm{CMB,c}}/C_{\mathrm{CMB,m}}$ and by the flux balance condition

$$\varrho_{\mathrm{c}} \kappa_{\mathrm{H,c}} \left.\frac{\partial C_{\mathrm{c}}}{\partial x}\right|_{x=-0} = \varrho_{\mathrm{m}} \kappa_{\mathrm{H,m}} \left.\frac{\partial C_{\mathrm{m}}}{\partial x}\right|_{x=+0}, \tag{A.2}$$

and the solution for the mantle side ($x > 0$) is (Zhang, 2008, pp. 204f.):

$$C_{\mathrm{m}}(x,t) = C_{\mathrm{m},\infty} + \frac{(D^{\mathrm{H}}_{\mathrm{Fe/rw}} C_{\mathrm{c},\infty} - C_{\mathrm{m},\infty})}{1 + D^{\mathrm{H}}_{\mathrm{Fe/rw}} \gamma} \operatorname{erfc}\left(\frac{x}{2\sqrt{\kappa_{\mathrm{H,m}} t}}\right), \tag{A.3}$$

where $C_{\mathrm{c},\infty}$ and $C_{\mathrm{m},\infty}$ are the initially homogeneous concentrations in the core and mantle and $\gamma = (\varrho_{\mathrm{m}}/\varrho_{\mathrm{c}})\sqrt{\kappa_{\mathrm{H,m}}/\kappa_{\mathrm{H,c}}}$.

In the actual planet, hydrogen will not be transported only by diffusion, especially in the core, which convects many orders of magnitude more rapidly than the mantle. We include this rapid transport by treating $\kappa_{\mathrm{H,c}}$ as an "effective diffusivity" that is much higher than the actual diffusivity. We use $\varrho_{\mathrm{m}} = 4100\ \mathrm{kg/m^3}$ and $\varrho_{\mathrm{c}} = 6450\ \mathrm{kg/m^3}$. The diffusivity of hydrogen in ringwoodite has been found to be lower by about a factor 30 than the diffusivity in polycrystalline wadsleyite (Kudo et al., 2006), for which Hae et al. (2006) determined $\kappa_{\mathrm{H}} = 9.6 \times 10^{-6} \exp[-123\ \mathrm{kJ/mol}/(RT)]$ at 15 GPa. We find that for a temperature of 2100 K on the mantle side of the CMB and $\kappa_{\mathrm{H,c}} = 1000\kappa_{\mathrm{H,m}}$, it takes ~3.5 Gy for a shell around the core with less than 80% of the initial water content to grow to a thickness of 10 km (corresponding to 0.25% of the total volume of the mantle) even if the core initially had the same H concentration as the mantle. However, as the core would have absorbed a large amount of hydrogen during core formation, the shell will grow even more slowly at the later stages considered in this paper. For an already enriched core and an assumed residence time for a parcel of mantle material at the CMB of ~150 My, the shell may be less than 1 km thick. If the base of the martian mantle is solid, which is quite possible at least for the later stages of martian evolution in water-poor models, it is therefore unlikely that any substantial fraction of the martian mantle experiences hydrogen loss to the core after core formation. Even if the lowermost mantle is partially molten, it is not at all clear whether hydrogen exchange between silicate and metal melts would have a similar dehydrating effect on the mantle and whether the density relations in the silicate melt are conducive to advective transport of hydrogen over larger distances than diffusion with percolating silicate melts. Therefore we consider it acceptable to neglect this effect in our models. Moreover, even if ancient subducted lithosphere existed at the martian CMB and remained there for several billion years, it may have lost only a minor part of its water to the core, because it is even less likely to be molten than normal mantle due to its low temperature.

Appendix B. Supplementary data

Supplementary data associated with this article can be found, in the online version, at http://dx.doi.org/10.1016/j.pepi.2013.04.006.

References

Agee, C.B., 2008. Compressibility of water in magma and the prediction of density crossovers in mantle differentiation. Philos. Trans. R. Soc. A366, 4239–4252.

Agee, C.B., Wilson, N.V., McCubbin, F.M., Ziegler, K., Polyak, V.J., Sharp, Z.D., Asmerom, Y., Nunn, M.H., Shaheen, R., Thiemens, M.H., Steele, A., Fogel, M.L., Bowden, R., Glamoclija, M., Zhang, Z., Elardo, S.M., 2013. Unique meteorite from early Amazonian Mars: water-rich basaltic breccia Northwest Africa 7034. Science 339, 780–785.

Arkani-Hamed, J., 2005. Magnetic crust of Mars. J. Geophys. Res. 110, E08005. http://dx.doi.org/10.1029/2004JE002397.

Aubaud, C., Hauri, E.H., Hirschmann, M.M., 2004. Hydrogen partition coefficients between nominally anhydrous minerals and basaltic melts. Geophys. Res. Lett. 31, L20611. http://dx.doi.org/10.1029/2004GL021341.

Avé Lallemant, H.G., Carter, N.L., 1970. Syntectonic recrystallization of olivine and modes of flow in the upper mantle. Geol. Soc. Am. Bull. 81, 2203–2220.

Banerdt, W.B., Smrekar, S., Alkalai, L., Hoffman, T., Warwick, R., Hurst, K., Folkner, W., Lognonné, P., Spohn, T., Asmar, S., Banfield, D., Boschi, L., Christensen, U., Dehant, V., Giardini, D., Goetz, W., Golombek, M., Grott, M., Hudson, T., Johnson, C., Kargl, G., Kobayashi, N., Maki, J., Mimoun, D., Mocquet, A., Morgan, P., Panning, M., Pike, W.T., Tromp, J., van Zoest, T., Weber, R., Wieczorek, M., InSight Team, 2012. InSight: An Integrated Exploration of the Interior of Mars. Lunar Planet. Sci. XLIII, Abstract 2838.

Baratoux, D., Toplis, M.J., Monnereau, M., Gasnault, O., 2011. Thermal history of Mars inferred from orbital geochemistry of volcanic provinces. Nature 472, 338–341, Correction in 475, 254.

Bercovici, D., Karato, S.-i., 2003. Whole-mantle convection and the transition-zone water filter. Nature 425, 39–44.

Bertka, C.M., Fei, Y., 1997. Mineralogy of the Martian interior up to core–mantle boundary pressures. J. Geophys. Res. 102, 5251–5264.

Bertka, C.M., Holloway, J.R., 1994. Anhydrous partial melting of an iron-rich mantle I: subsolidus phase assemblages and partial melting phase relations at 10 to 30 kbar. Contrib. Mineral. Petrol. 115, 313–322.

Bills, B.G., Neumann, G.A., Smith, D.E., Zuber, M.T., 2005. Improved estimate of tidal dissipation within Mars from MOLA observations of the shadow of Phobos. J. Geophys. Res. 110, E07004. http://dx.doi.org/10.1029/2004JE002376.

Blundy, J., Wood, B., 2003. Mineral–melt partitioning of uranium, thorium and their daughters. In: Bourdon, B., Henderson, G.M., Lundstrom, C.C., Turner, S.P. (Eds.), Uranium-series Geochemistry, no. 52 in Rev. Mineral. Geochem. Mineralogical Society of America, Washington, D.C, pp. 59–123.

Boctor, N.Z., Alexander, C.M.O., Wang, J., Hauri, E., 2003. The sources of water in Martian meteorites. Geochim. Cosmochim. Acta 67, 3971–3989.

Bolfan-Casanova, N., Keppler, H., Rubie, D.C., 2000. Water partitioning between nominally anhydrous minerals in the MgO–SiO_2–H_2O system up to 24 GPa: implications for the distribution of water in the Earth's mantle. Earth Planet. Sci. Lett. 182, 209–221.

Bolfan-Casanova, N., Keppler, H., Rubie, D.C., 2003. Water partitioning at 660 km depth and evidence for very low water solubility in magnesium silicate perovskite. Geophys. Res. Lett. 30, 1905. http://dx.doi.org/10.1029/2003GL017182.

Borg, L., Nyquist, L.E., Taylor, L.A., Weismann, H., Shih, C.-Y., 1997. Constraints on Martian differentiation processes from Rb–Sr and Sm–Nd isotopic analyses of the basaltic shergottite QUE 94201. Geochim. Cosmochim. Acta 61, 4915–4931.

Boyce, J.M., Mouginis-Mark, P., Garbeil, H., 2005. Ancient oceans in the northern lowlands of Mars: evidence from impact crater depth/diameter relationships. J. Geophys. Res. 110, E03008. http://dx.doi.org/10.1029/2004JE002328.

Boynton, W.V., Taylor, G.J., Karunatillake, S., Reedy, R.C., Keller, J.M., 2008. Elemental abundances determined via the Mars Odyssey GRS. In: Bell, J.F., III (Ed.), The Martian Surface: Composition, Mineralogy, and Physical Properties. Cambridge University Press, pp. 105–124.

Brain, D.A., Jakosky, B.M., 1998. Atmospheric loss since the onset of the Martian geologic record: combined role of impact erosion and sputtering. J. Geophys. Res. 103, 22689–22694.

Brandon, A.D., Walker, R.J., Morgan, J.W., Gates, G.G., 2000. Re–Os isotopic evidence for early differentiation of the martian mantle. Geochim. Cosmochim. Acta 64, 4083–4095.

Braun, M.G., Hirth, G., Parmentier, E.M., 2000. The effect of deep damp melting on mantle flow and melt generation beneath mid-ocean ridges. Earth Planet. Sci. Lett. 176, 339–356.

Breuer, D., Spohn, T., 2006. Viscosity of the Martian mantle and its initial temperature: constraints from crust formation history and the evolution of the magnetic field. Planet. Space Sci. 54, 153–169.

Carr, M.H., Head III, J.W., 2003. Oceans on Mars: an assessment of the observational evidence and possible fate. J. Geophys. Res. 108, 5042. http://dx.doi.org/10.1029/2002JE001963.

Carr, M.H., Head III, J.W., 2010. Geologic history of Mars. Earth Planet. Sci. Lett. 294, 185–203.

Cassata, W.S., Shuster, D.L., Renne, P.R., Weiss, B.P., 2012. Trapped Ar isotopes in meteorite ALH 84001 indicate Mars did not have a thick ancient atmosphere. Icarus 221, 461–465.

Chen, J., Inoue, T., Weidner, D.J., Wu, Y., Vaughan, M.T., 1998. Strength and water weakening of mantle minerals, olivine, wadsleyite and ringwoodite. Geophys. Res. Lett. 25, 575–578, Correction in 25(7), pp. 1103–1104.

Chen, J.H., Wasserburg, G.J., 1986. Formation ages and evolution of Shergotty and its parent planet from U–Th–Pb systematics. Geochim. Cosmochim. Acta 50, 955–968.

Cheung, K.K., King, S.D., 2011. Using crustal thickness modeling to study Mars' crustal/mantle structures. Lunar Planet. Sci. XLII, Abstract 1534.

Christensen, P.R., 2006. Water at the poles and in permafrost regions of Mars. Elements 2, 151–155.

Clifford, S.M., 1993. A model for the hydrologic and climatic behavior of water on Mars. J. Geophys. Res. 98, 10973–11016.

Clifford, S.M., Parker, T.J., 2001. The evolution of the martian hydrosphere: Implications for the fate of a primordial ocean and the current state of the northern plains. Icarus 154, 40–79.

Dann, J.C., Holzheid, A.H., Grove, T.L., McSween, H.Y., 2001. Phase equilibria of the Shergotty meteorite: constraints on pre-eruptive water contents of martian magmas and fractional crystallization under hydrous conditions. Meteorit. Planet. Sci. 36, 793–806.

Davies, J.H., Bickle, M.J., 1991. A physical model for the volume and composition of melt produced by hydrous fluxing above subduction zones. Philos. Trans. R. Soc. A 335, 355–364.

Defraigne, P., Dehant, V., van Hoolst, T., 2001. Steady-state convection in Mars' mantle. Planet. Space Sci. 49, 501–509.

Draper, D.S., Xirouchakis, D., Agee, C.B., 2003. Trace element partitioning between garnet and chondritic melt from 5 to 9 GPa: implications for the onset of the majorite transition in the martian mantle. Earth Planet. Sci. Lett. 139, 149–169.

Dreibus, G., Spettel, B., Wlotzka, F., Schultz, L., Weber, H.W., Jochum, K.P., Wänke, H., 1996. QUE94201: an unusual Martian basalt. Meteorit. Planet. Sci. 31, A39–A40.

Elkins-Tanton, L.T., 2008. Linked magma ocean solidification and atmospheric growth for Earth and Mars. Earth Planet. Sci. Lett. 271, 181–191.

Elkins-Tanton, L.T., Parmentier, E.M., Hess, P.C., 2003. Magma ocean fractional crystallization and cumulate overturn in terrestrial planets: implications for Mars. Meteorit. Planet. Sci. 38, 1753–1771.

Faul, U.H., 2001. Melt retention and segregation beneath mid-ocean ridges. Nature 410, 920–923.

Fei, Y., Van Orman, J., Li, J., van Westrenen, W., Sanloup, C., Minarik, W., Hirose, K., Komabayashi, T., Walter, M.J., Funakoshi, K.-i., 2004. Experimentally determined postspinel transformation boundary in Mg_2SiO_4 using MgO as an internal pressure standard and its geophysical implications. J. Geophys. Res. 109, B02305. http://dx.doi.org/10.1029/2003JB002562.

Filiberto, J., Dasgupta, R., 2011. Fe^{2+}–Mg partitioning between olivine and basaltic melts: applications to genesis of olivine-phyric shergottites and conditions of melting in the Martian interior. Earth Planet. Sci. Lett. 304, 527–537.

Filiberto, J., Dasgupta, R., Kiefer, W.S., Treiman, A.H., 2010. High pressure, near-liquidus phase equilibria of the Home Plate basalt Fastball and melting in the martian mantle. Geophys. Res. Lett. 37, L13201. http://dx.doi.org/10.1029/2010GL043999.

Gaetani, G.A., Grove, T.L., 1998. The influence of water on melting of mantle peridotite. Contrib. Mineral. Petrol. 131, 323–346.

Gasparik, T., 2003. Phase Diagrams for Geoscientists. Springer, Berlin, 462 pp.

Ghods, A., Arkani-Hamed, J., 2011. Effects of the Borealis impact on the mantle dynamics of Mars. Phys. Earth Planet. Inter. 188, 37–46.

Golabek, G.J., Keller, T., Gerya, T.V., Zhu, G., Tackley, P.J., Connolly, J.A.D., 2011. Origin of the martian dichotomy and Tharsis from a giant impact causing massive magmatism. Icarus 215, 346–357.

Grant, K., Ingrin, J., Lorand, J.P., Dumas, P., 2007. Water partitioning between mantle minerals from peridotite xenoliths. Contrib. Mineral. Petrol. 154, 15–34.

Griggs, D.T., Blačić, J.D., 1965. Quartz: anomalous weakness of synthetic crystals. Science 147, 292–295.

Grott, M., Morschhauser, A., Breuer, D., Hauber, E., 2011. Volcanic outgassing of CO_2 and H_2O on Mars. Earth Planet. Sci. Lett. 308, 391–400.

Hae, R., Ohtani, E., Kubo, T., Koyama, T., Utada, H., 2006. Hydrogen diffusivity in wadsleyite and water distribution in the mantle transition zone. Earth Planet. Sci. Lett. 243, 141–148.

Hahn, B.C., McLennan, S.M., 2010. Regional martian crustal heat flow from Mars Odyssey gamma-ray spectrometry. Lunar Planet. Sci. XLI, Abstract 1371.

Harlow, G.E., 1997. K in clinopyroxene a high pressure and temperature: an experimental study. Am. Mineral. 82, 259–269.

Hauck, S.A., Phillips, R.J., 2002. Thermal and crustal evolution of Mars. J. Geophys. Res. 107, 5052. http://dx.doi.org/10.1029/2001JE001801.

Hauri, E.H., Gaetani, G.A., Green, T.H., 2006. Partitioning of water during melting of the Earth's upper mantle at H_2O-undersaturated conditions. Earth Planet. Sci. Lett. 248, 715–734.

Hauri, E.H., Wagner, T.P., Grove, T.L., 1994. Experimental and natural partitioning of Th, U, Pb and other trace elements between garnet, clinopyroxene and basaltic melts. Chem. Geol. 117, 149–166.

Hernlund, J.W., Tackley, P.J., 2007. Some dynamical consequences of partial melting in Earth's deep mantle. Phys. Earth Planet. Inter. 162, 149–163.

Hernlund, J.W., Tackley, P.J., 2008. Modeling mantle convection in the spherical annulus. Phys. Earth Planet. Inter. 171, 48–54.

Hirose, K., Kawamoto, T., 1995. Hydrous partial melting of lherzolite at 1 GPa: the effect of H_2O on the genesis of basaltic magmas. Earth Planet. Sci. Lett. 133, 463–473.

Hirschmann, M.M., Asimow, P.D., Ghiorso, M.S., Stolper, E.M., 1999. Calculation of peridotite partial melting from thermodynamic models of minerals and melts. III. Controls on isobaric melt production and the effect of water on melt production. J. Petrol. 40, 831–851.

Hirth, G., Kohlstedt, D.L., 1996. Water in the oceanic upper mantle: implications for rheology, melt extraction and evolution of the lithosphere. Earth Planet. Sci. Lett. 144, 93–108.

Hirth, G., Kohlstedt, D.L., 2003. Rheology of the upper mantle and the mantle wedge: a view from the experimentalists. In: Eiler, J. (Ed.), Inside the Subduction Factory, Geophysical Monograph, vol. 138. American Geophysical Union, Washington, D.C, pp. 83–105.

Hofmeister, A.M., Branlund, J.M., Pertermann, M., 2007. Properties of rocks and minerals – Thermal conductivity of the Earth. In: Price, G.D. (Ed.), Mineral Physics, vol. 2 of Treatise on Geophysics. Elsevier, pp. 543–577.

Ito, E., Takahashi, E., 1989. Postspinel transformations in the system Mg_2SiO_4–Fe_2SiO_4 and some geophysical implications. J. Geophys. Res. 94, 10637–10646.

Ito, G., Shen, Y., Hirth, G., Wolfe, C.J., 1999. Mantle flow, melting and dehydration of the Iceland mantle plume. Earth Planet. Sci. Lett. 165, 81–96.

Jaupart, C., Mareschal, J.-C., 2003. Constraints on crustal heat production from heat flow data. In: Rudnick, R.L. (Ed.), The Crust, vol. 3 of Treatise on Geochemistry. Elsevier, pp. 65–84.

Jin, Z.-M., Zhang, J., Green II, H.W., Jin, S., 2001. Eclogite rheology: implications for subducted lithosphere. Geology 29, 667–670.

Jing, Z., Karato, S.-i., 2009. The density of volatile bearing melts in the Earth's deep mantle: the role of chemical composition. Chem. Geol. 262, 100–107.

Karato, S.-I., 2008. Deformation of Earth Materials. Cambridge University Press, x+463 pp.

Karato, S.-I., Paterson, M.S., Fitz Gerald, J.D., 1986. Rheology of synthetic olivine aggregates: influence of grain size and water. J. Geophys. Res. 91, 8151–8176.

Karato, S.-I., Wu, P., 1993. Rheology of the upper mantle: a synthesis. Science 260, 771–778.

Katsura, T., Ito, E., 1989. The system Mg_2SiO_4–Fe_2SiO_4 at high pressures and temperatures: Precise determination of stabilities of olivine, modified spinel, and spinel. J. Geophys. Res. 94, 15663–15670.

Katsura, T., Yamada, H., Nishikawa, O., Song, M., Kubo, A., Shinmei, T., Yokoshi, S., Aizawa, Y., Yoshino, T., Walter, M.J., Ito, E., Funakoshi, K.-i., 2004. Olivine–wadsleyite transition in the system $(Mg, Fe)_2SiO_4$. J. Geophys. Res. 109, B02209. http://dx.doi.org/10.1029/2003JB002438.

Katz, R.F., Spiegelman, M., Langmuir, C., 2003. A new parameterization of hydrous mantle melting. Geochem. Geophys. Geosyst. 4, 1073. http://dx.doi.org/10.1029/2002GC000433.

Keller, T., Tackley, P.J., 2009. Towards self-consistent modeling of the martian dichotomy: the influence of one-ridge convection on crustal thickness distribution. Icarus 202, 429–443.

Kiefer, W.S., 2003. Melting in the martian mantle: shergottite formation and implications for present-day mantle convection on Mars. Meteorit. Planet. Sci. 38, 1815–1832.

Kiefer, W.S., Bills, B.G., Nerem, R.S., 1996. An inversion of gravity and topography for mantle and crustal structure on Mars. J. Geophys. Res. 101, 9239–9252.

Kohlstedt, D.L., Bai, Q., Wang, Z.-C., Mei, S., 2000. Rheology of partially molten rocks. In: Bagdassarov, N., Laporte, D., Thompson, A.B. (Eds.), Physics and Chemistry of Partially Molten Rocks. Kluwer Academic Publishers, Dordrecht, The Netherlands, pp. 3–28.

Kohlstedt, D.L., Keppler, H., Rubie, D.C., 1996. Solubility of water in the α, β and γ phases of (Mg, Fe)2SiO4. Contrib. Mineral. Petrol. 123, 345–357.

Kohn, S.C., Grant, K.J., 2006. The partitioning of water between nominally anhydrous minerals and silicate melts. In: Keppler, H., Smyth, J.R. (Eds.), Water in Nominally Anhydrous Minerals, no. 62 in Rev. Mineral. Geochem. Mineralogical Society of America, Washington, D.C, pp. 231–241.

Konopliv, A.S., Asmar, S.W., Folkner, W.M., Karatekin, Ö., Nunes, D.C., Smrekar, S.E., Yoder, C.F., Zuber, M.T., 2011. Mars high resolution gravity fields from MRO, Mars seasonal gravity, and other dynamical parameters. Icarus 211, 401–428.

Konopliv, A.S., Yoder, C.S., Standish, E.M., Yuan, D.-N., Sjogren, W.L., 2006. A global solution for the Mars static and seasonal gravity, Mars orientation, Phobos and Deimos masses, and Mars ephemeris. Icarus 182, 32–50.

Krasnopolsky, V. 2000. On the deuterium abundance on Mars and some related problems. Icarus 148, 597–602. Erratum in 150, 194 (2001).

Kubo, T., Ohtani, E., Kato, T., Shinmei, T., Fujino, K., 1998. Effects of water on the α–β transformation kinetics in San Carlos olivine. Science 281, 85–87.

Kudo, T., Ohtani, E., Hae, R., Shimojuku, A., 2006. Diffusion of hydrogen in ringwoodite. In: Saad, Z. (Ed.), Conf. Proc, vol. 833. American Institute of Physics, New York, pp. 148–149.
Kusanagi, T., Matsui, T., 2000. The change of eruption styles of Martian volcanoes and estimates of the water content of the Martian mantle. Phys. Earth Planet. Inter. 117, 437–447.
Kushiro, I., 1969. The system forsterite–diopside–silica with and without water at high pressures. Am. J. Sci. A267, 269–294.
Kushiro, I., Yoder Jr., H.S., Nishikawa, M., 1968. Effect of water on the melting of enstatite. Geol. Soc. Am. Bull. 79, 1685–1692.
Lammer, H., Lichtenegger, H.I.M., Kolb, C., Ribas, I., Guinan, E.F., Abart, R., Bauer, S.J., 2003. Loss of water from Mars: implications for the oxidation of the soil. Icarus 165, 9–25.
Lasue, J., Mangold, N., Hauber, E., Clifford, S., Feldman, W., Gasnault, O., Grima, C., Maurice, S., Mousis, O., 2013. Quantitative assessments of the martian hydrosphere. Space Sci. Rev. 174, 155–212.
Leone, G., Wilson, L., Davies, A.G., 2011. The geothermal gradient of Io: consequences for lithosphere structure and volcanic eruptive activity. Icarus 211, 623–635.
Leshin, L.A., 2000. Insights into martian water reservoirs from analyses of martian meteorite QUE94201. Geophys. Res. Lett. 27, 2017–2020.
Lewis, K.W., Simons, F.J., 2012. Local spectral variability and the origin of the Martian crustal magnetic field. Geophys. Res. Lett. 39, L18201. http://dx.doi.org/10.1029/2012GL052708.
Li, Q., Kiefer, W.S., 2007a. Mantle convection and magma production on present-day Mars: effects of temperature-dependent rheology. Geophys. Res. Lett. 34, L16203. http://dx.doi.org/10.1029/2007GL030544.
Li, Q., Kiefer, W.S., 2007b. Mantle convection and magma production on present-day Mars: the effects of water. Lunar Planet. Sci. XXXVIII, Abstract 2062.
Litasov, K.D., Ohtani, E., 2007. Effect of water on the phase relations in Earth's mantle and deep water cycle. In: Ohtani, E. (Ed.), Advances in High-Pressure Mineralogy, Special Paper 421. Geological Society of America, Boulder, Colorado, pp. 115–146.
Lodders, K., Fegley Jr., B., 1997. An oxygen isotope model for the composition of Mars. Icarus 126, 373–394.
Mackwell, S.J., Zimmerman, M.E., Kohlstedt, D.L., 1998. High-temperature deformation of dry diabase with application to tectonics on Venus. J. Geophys. Res. 103, 975–984.
Manga, M., 1996. Mixing of heterogeneities in the mantle: effect of viscosity differences. Geophys. Res. Lett. 23, 403–406.
Manga, M., Patel, A., Dufek, J., Kite, E.S., 2012. Wet surface and dense atmosphere on early Mars suggested by the bomb sag at Home Plate. Mars. Geophys. Res. Lett. 39, L01202. http://dx.doi.org/10.1029/2011GL050192.
Marinova, M.M., Aharonson, O., Asphaug, E., 2008. Mega-impact formation of the Mars hemispheric dichotomy. Nature 453, 1216–1219.
Marty, B., Balmino, G., Duron, J., Rosenblatt, P., Le Maistre, S., Rivoldini, A., Dehant, V., Van Hoolst, T., 2009. Martian gravity field model and its time variations from MGS and Odyssey data. Planet. Space Sci. 57, 350–363.
McCubbin, F.M., Hauri, E.H., Elardo, S.M., Vander Kaaden, K.E., Wang, J., Shearer Jr., C.K., 2012. Hydrous melting of the martian mantle produced both depleted and enriched shergottites. Geology 40, 683–686.
McCubbin, F.M., Smirnov, A., Nekvasil, H., Wang, J., Hauri, E., Lindsley, D.H., 2010. Hydrous magmatism on Mars: a source for water for the surface and subsurface during the Amazonian. Earth Planet. Sci. Lett. 292, 132–138.
McGovern, P.J., Solomon, S.C., Smith, D.E., Zuber, M.T., Simons, M., Wieczorek, M.A., Phillips, R.J., Neumann, G.A., Aharonson, O., Head, J.W., 2002. Localized gravity/topography admittance and correlation spectra on Mars: implications for regional and global evolution. J. Geophys. Res. 107, 5136. http://dx.doi.org/10.1029/2002JE001854, Correction in 109, E07007, 10.1029/2004JE002286 (2004).
McLennan, S.M., 2001. Crustal heat production and the thermal evolution of Mars. Geophys. Res. Lett. 28, 4019–4022.
McSween, H.Y., Grove, T.L., Lentz, R.C.F., Dann, J.C., Holzheid, A.H., Riciputi, L.R., Ryan, J.G., 2001. Geochemical evidence for magmatic water within Mars from pyroxenes in the Shergotty meteorite. Nature 409, 487–490.
McSween Jr., H.Y., 2003. Mars. In: Davis, A.M. (Ed.), Meteorites, Comets, and Planets, vol. 1 of Treatise on Geochemistry. Elsevier, pp. 601–621.
Médard, E., Grove, T.L., 2006. Early hydrous melting and degassing of the Martian interior. J. Geophys. Res. 111, E11003. http://dx.doi.org/10.1029/2006JE002742.
Mibe, K., Orihashi, Y., Nakai, S., Fujii, T., 2006. Element partitioning between transition-zone minerals and ultramafic melt under hydrous conditions. Geophys. Res. Lett. 33, L16307. http://dx.doi.org/10.1029/2006GL026999.
Montési, L.G.J., Zuber, M.T., 2003. Clues to the lithospheric structure of Mars from wrinkle ridge sets and localization instability. J. Geophys. Res. 108, 5048. http://dx.doi.org/10.1029/2002JE001974.
Morschhauser, A., Grott, M., Breuer, D., 2011. Crustal recycling, mantle dehydration, and the thermal evolution of Mars. Icarus 212, 541–558.
Nahm, A.L., Schultz, R.A., 2011. Magnitude of global contraction on Mars from analysis of surface faults: implications for martian thermal history. Icarus 211, 389–400.
Neukum, G., Basilevsky, A.T., Kneissl, T., Chapman, M.G., van Gasselt, S., Michael, G., Jaumann, R., Hofmann, H., Lanz, J.K., 2010. The geologic evolution of Mars: episodicity of resurfacing events and ages from cratering analysis of image data and correlation with radiometric ages of Martian meteorites. Earth Planet. Sci. Lett. 294, 204–222.
Neumann, G.A., Zuber, M.T., Wieczorek, M.A., McGovern, P.J., Lemoine, F.G., Smith, D.E., 2004. Crustal structure of Mars from gravity and topography. J. Geophys. Res. 109, E08002. http://dx.doi.org/10.1029/2004JE002262.
Newsom, H.E., Crumpler, L.S., Reedy, R.C., Petersen, M.T., Newsom, G.C., Evans, L.G., Taylor, G.J., Keller, J.M., Janes, D.M., Boynton, W.V., Kerry, K.E., Karunatillake, S., 2007. Geochemistry of Martian soil and bedrock in mantled and less mantled terrains with gamma ray data from Mars Odyssey. J. Geophys. Res. 112, E03S12. http://dx.doi.org/10.1029/2006JE002680.
Nimmo, F., Gilmore, M.S., 2001. Constraints on the depth of magnetized crust on Mars from impact craters. J. Geophys. Res. 106, 12315–12323.
Nimmo, F., Hart, S.D., Korycansky, D.G., Agnor, C.B., 2008. Implications of an impact origin for the martian hemispheric dichotomy. Nature 453, 1220–1223.
Nimmo, F., Price, G.D., Brodholt, J., Gubbins, D., 2004. The influence of potassium on core and geodynamo evolution. Geophys. J. Int. 156, 363–376.
Nimmo, F., Stevenson, D.J., 2001. Estimates of Martian crustal thickness from viscous relaxation of topography. J. Geophys. Res. 106, 5085–5098.
Norman, M.D., 1999. The composition and thickness of the crust of Mars estimated from rare earth elements and neodymium-isotopic compositions of Martian meteorites. Meteorit. Planet. Sci. 34, 439–449.
Norman, M.D., 2002. Thickness and composition of the martian crust revisited: implications of an ultradepleted mantle with a Nd isotopic composition like that of QUE94201. Lunar Planet. Sci. XXXIII, Abstract 1175.
Ogawa, M., Yanagisawa, T., 2011. Numerical models of Martian mantle evolution induced by magmatism and solid-state convection beneath stagnant lithosphere. J. Geophys. Res. 116, E08008. http://dx.doi.org/10.1029/2010JE003777.
Ogawa, M., Yanagisawa, T., 2012. Two-dimensional numerical studies on the effects of water on Martian mantle evolution induced by magmatism and solid-state mantle convection. J. Geophys. Res. 117, E06004. http://dx.doi.org/10.1029/2012JE004054.
O'Neill, C.J., Lenardic, A., Jellinek, A.M., Kiefer, W.S., 2007. Melt propagation and volcanism in mantle convection simulations, with applications for Martian volcanic and atmospheric evolution. J. Geophys. Res. 112, E07003. http://dx.doi.org/10.1029/2006JE002799.
Phillips, R.J., Zuber, M.T., Smrekar, S.E., Mellon, M.T., Head, J.W., Tanaka, K.L., Putzig, N.E., Milkovich, S.M., Campbell, B.A., Plaut, J.J., Safaeinili, A., Seu, R., Biccari, D., Carter, L.M., Picardi, G., Orosei, R., Mohit, P.S., Heggy, E., Zurek, R.W., Egan, A.F., Giacomoni, E., Russo, F., Cutigni, M., Pettinelli, E., Holt, J.W., Leuschen, C.J., Marinangeli, L., 2008. Mars north polar deposits: stratigraphy, age, and geodynamical response. Science 320, 1182–1185.
Phillips, R.J., Zuber, M.T., Solomon, S.C., Golombek, M.P., Jakosky, B.M., Banerdt, W.B., Smith, D.E., Williams, R.M.E., Hynes, B.M., Aharonson, O., Hauck II, S.A., 2001. Ancient geodynamics and global-scale hydrology on Mars. Science 291, 2587–2591.
Phipps Morgan, J., 1997. The generation of a compositional lithosphere by mid-ocean ridge melting and its effect on subsequent off-axis hotspot upwelling and melting. Earth Planet. Sci. Lett. 146, 213–232.
Plesa, A.-C., Breuer, D., 2011. Thermo-chemical evolution of a one-plate planet: Application to Mars. EPSC Abstracts 6, EPSC-DPS2011-1286.
Poulet, F., Mangold, N., Platevoet, B., Bardintzeff, J.-M., Sautter, V., Mustard, J.F., Bibring, J.-P., Pinet, P., Langevin, Y., Gondet, B., Aléon-Toppani, A., 2009. Quantitative compositional analysis of martian mafic regions using the MEx/OMEGA reflectance data: 2. Petrological implications. Icarus 201, 84–101.
Ravat, D., 2011. Interpretation of Mars southern highlands high amplitude magnetic field with total gradient and fractal source modeling: new insights into the magnetic mystery of Mars. Icarus 214, 400–412.
Reese, C.C., Solomatov, V.S., Baumgardner, J.R., Stegman, D.R., Vezolainen, A.V., 2004. Magmatic evolution of impact-induced Martian mantle plumes and the origin of Tharsis. J. Geophys. Res. 109, E08009. http://dx.doi.org/10.1029/2003JE002222.
Robbins, S.J., Di Achille, G., Hynek, B.M., 2011. The volcanic history of Mars: high-resolution crater-based studies of the calderas of 20 volcanoes. Icarus 211, 1179–1203.
Roberts, J.H., Arkani-Hamed, J., 2012. Impact-induced mantle dynamics on Mars. Icarus 218, 278–289.
Roberts, J.H., Zhong, S., 2006. Degree-1 convection in the Martian mantle and the origin of the hemispheric dichotomy. J. Geophys. Res. 111, E06013. http://dx.doi.org/10.1029/2005JE002668.
Ruedas, T., 2006. Dynamics, crustal thicknesses, seismic anomalies, and electrical conductivities in dry and hydrous ridge-centered plumes. Phys. Earth Planet. Inter. 155, 16–41.
Ruedas, T., Tackley, P.J., Solomon, S.C., 2009. Water, melting, and convection in the martian mantle. Lunar Planet. Sci. XL, Abstract 1463.
Ruedas, T., Tackley, P.J., Solomon, S.C., 2013. Thermal and compositional evolution of the martian mantle: effects of phase transitions and melting. Phys. Earth Planet. Inter. 216, 32–58.
Ruiz, J., Fernández, C., Gomez-Ortiz, D., Dohm, J.M., López, V., Tejero, R., 2008. Ancient heat flow, crustal thickness, and lithospheric mantle rheology in the Amenthes region, Mars. Earth Planet. Sci. Lett. 270, 1–12.
Ruiz, J., López, V., Dohm, J.M., 2010. The present-day thermal state of Mars. Icarus 207, 631–637.
Ruiz, J., McGovern, P.J., Jiménez-Dıaz, A., López, V., Williams, J.-P., Hahn, B.C., Tejero, R., 2011. The thermal evolution of Mars as constrained by paleo-heat flows. Icarus 215, 508–517.
Ruiz, J., McGovern, P.J., Tejero, R., 2006. The early thermal and magnetic state of the cratered highlands of Mars. Earth Planet. Sci. Lett. 241, 2–10.

Saal, A.E., Hauri, E.H., Langmuir, C.H., Perfit, M.R., 2002. Vapour undersaturation in primitive mid-ocean-ridge basalt and the volatile content of Earth's upper mantle. Nature 419, 451–455.

Sakane, S., Liu, W., Doren, D.J., Shock, E.L., Wood, R.H., 2001. Prediction of the Gibbs energies and an improved equation of state for water at extreme conditions from ab initio energies with classical simulations. Geochim. Cosmochim. Acta 65, 4067–4075, Correction in vol. 66(24), p. 4365.

Sanloup, C., Jambon, A., Gillet, P., 1999. A simple chondritic model of Mars. Phys. Earth Planet. Inter. 112, 43–54.

Saxena, S.K., Chatterjee, N., Fei, Y., Shen, G., 1993. Thermodynamic Data on Oxides and Silicates. Springer, Berlin, 428 pp.

Schmalzl, J., Houseman, G.A., Hansen, U., 1996. Mixing in vigorous, time-dependent three-dimensional convection and application to Earth's mantle. J. Geophys. Res. 101, 21847–21858.

Schmerr, N.C., Fei, Y., Bertka, C., 2001. Extending the solidus for a model iron-rich martian mantle composition to 25 GPa. Lunar Planet. Sci. XXXII, Abstract 1157.

Schumacher, S., Breuer, D., 2006. Influence of a variable thermal conductivity on the thermochemical evolution of Mars. J. Geophys. Res. 111, E02006, doi:10.1029/2006JE002755 2006.

Shibazaki, Y., Ohtani, E., Terasaki, H., Suzuki, A., Funakoshi, K.-i., 2009. Hydrogen partitioning between iron and ringwoodite: implications for water transport into the Martian core. Earth Planet. Sci. Lett. 287, 463–470.

Shimoda, G., Ikeda, Y., Kita, N.T., Morishita, Y., Imae, N., 2005. Two-stage plume melting: a possible mechanism for the origin of martian magmatism. Earth Planet. Sci. Lett. 235, 469–479.

Smith, D.E., Zuber, M.T., Solomon, S.C., Phillips, R.J., Head, J.W., Garvin, J.B., Banerdt, W.B., Muhleman, D.O., Pettengill, G.H., Neumann, G.A., Lemoine, F.G., Abshire, J.B., Aharonson, O., Brown, C.D., Hauck, S.A., Ivanov, A.B., McGovern, P.J., Zwally, H.J., Duxbury, T.H., 1999. The global topography of Mars and implications for surface evolution. Science 284, 1495–1503.

Sohl, F., Spohn, T., 1997. The interior structure of Mars: implications from SNC meteorites. J. Geophys. Res. 102, 1613–1636.

Spence, D.A., Ockendon, J.R., Wilmott, P., Turcotte, D.L., Kellogg, L.H., 1988. Convective mixing in the mantle: the role of viscosity differences. Geophys. J. 95, 79–86.

Spohn, T., Grott, M., Knollenberg, J., van Zoest, T., Kargl, G., Smrekar, S.E., Banerdt, W.B., Hudson, T.L., HP^3 instrument team 2012. InSight: Measuring the martian heat flow using the Heat Flow and Physical Properties Package (HP^3). Lunar Planet. Sci. XLIII, Abstract 1445.

Steinberger, B., Werner, S.C., Torsvik, T.H., 2010. Deep vs. shallow origin of gravity anomalies, topography and volcanism on Earth, Venus and Mars. Icarus 207, 564–577.

Surkov, Y.A., Moskaleva, L.P., Zolotov, M.Y., Kharynkova, V.P., Manvelyan, O.S., Smirnov, G.G., Golovin, A.V., 1994. Phobos-2 data on martian surface geochemistry. Geochem. Int. 31, 50–58.

Tackley, P.J., 1996. Effects of strongly variable viscosity on three-dimensional compressible convection in planetary mantles. J. Geophys. Res. 101, 3311–3332.

Tackley, P.J., 2008. Modelling compressible mantle convection with large viscosity contrasts in a three-dimensional spherical shell using the yin-yang grid. Phys. Earth Planet. Inter. 171, 7–18.

Tackley, P.J., King, S.D., 2003. Testing the tracer ratio method for modeling active compositional fields in mantle convection simulations. Geochem. Geophys. Geosyst. 4, 8302. http://dx.doi.org/10.1029/2001GC000214.

Taylor, G.J., Boynton, W., Brückner, J., Wänke, H., Dreibus, G., Kerry, K., Keller, J., Reedy, R., Evans, L., Starr, R., Squyres, S., Karunatillake, S., Gasnault, O., Maurice, S., d'Uston, C., Englert, P., Dohm, J., Baker, V., Hamara, D., Janes, D., Sprague, A., Kim, K., Drake, D., 2006. Bulk composition and early differentiation of Mars. J. Geophys. Res. 111, E03S10. http://dx.doi.org/10.1029/2005JE002645.

Taylor, G.J., McLennan, S.M., McSween Jr., H.Y., Wyatt, M.B., Lentz, R.C.F., 2008. Implications of observed primary lithologies. In: Bell, J.F., III (Ed.), The Martian Surface: Composition, Mineralogy, and Physical Properties. Cambridge University Press, pp. 501–518.

Taylor, S.R., McLennan, S.M., 2009. Planetary Crusts. Cambridge University Press, 400 pp.

Trombka, J.I., Evans, L.G., Starr, R., Floyd, S.R., Squyres, S.W., Whelan, J.T., Bamford, G.J., Coldwell, R.L., Rester, A.C., Surkov, Y.A., Moskaleva, L.P., Kharyukova, V.P., Manvelyan, O.S., Zaitseva, S.Y., Smirnov, G.G., 1991. Analysis of Phobos mission gamma ray spectra from Mars: two approaches. Lunar Planet. Sci. XXII, 1415–1416.

Turcotte, D.L., Shcherbakov, R., Malamud, B.D., Kucinskas, A.B., 2002. Is the Martian crust also the Martian elastic lithosphere? J. Geophys. Res. 107, 5091. http://dx.doi.org/10.1029/2001JE001594.

van Thienen, P., 2007. Convective vigour and heat flow in chemically differentiated systems. Geophys. J. Int. 169, 747–766.

Voorhies, C., 2008. Thickness of the magnetic crust of Mars. J. Geophys. Res. 113, E04004. http://dx.doi.org/10.1029/2007JE002928.

Wänke, H., Dreibus, G., 1994. Chemistry and accretion history of Mars. Philos. Trans. R. Soc. Lond. A 349, 285–293.

Werner, S.C., 2009. The global martian volcanic evolutionary history. Icarus 201, 44–68.

Wieczorek, M.A., Zuber, M.T., 2004. Thickness of the Martian crust: improved constraints from geoid-to-topography ratios. J. Geophys. Res. 109, E01009. http://dx.doi.org/10.1029/2003JE002153.

Withers, A.C., Hirschmann, M.M., Tenner, T.J., 2011. The effect of Fe on olivine H_2O storage capacity: consequences for H_2O in the martian mantle. Am. Mineral. 96, 1039–1053.

Wood, B.J., 1995. The effect of H_2O on the 410-kilometer seismic discontinuity. Science 268, 75–76.

Xie, S., Tackley, P.J., 2004. Evolution of U–Pb and Sm–Nd systems in numerical models of mantle convection and plate tectonics. J. Geophys. Res. 109, B11204. http://dx.doi.org/10.1029/2004JB003176.

Zhang, Y., 2008. Geochemical Kinetics. Princeton University Press, xxv+631 pp.

Zhao, Y., Zimmerman, M.E., Kohlstedt, D.L., 2009. Effect of iron content on the creep behavior of olivine: 1. Anhydrous conditions. Earth Planet. Sci. Lett. 287, 229–240.

Zhao, Y.-H., Ginsberg, S.B., Kohlstedt, D.L., 2004. Solubility of hydrogen in olivine: dependence on temperature and iron content. Contrib. Mineral. Petrol. 147, 155–161.

Zhong, S., Zuber, M.T., 2001. Degree-1 mantle convection and the crustal dichotomy on Mars. Earth Planet. Sci. Lett. 189, 75–84.

Zuber, M.T., Smith, D.E., Solomon, S.C., Abshire, J.B., Afzal, R.S., Aharonson, O., Fishbaugh, K., Ford, P.G., Frey, H.V., Garvin, J.B., Head, J.W., Ivanov, A.B., Johnson, C.L., Muhleman, D.O., Neumann, G.A., Pettengill, G.H., Phillips, R.J., Sun, X., Zwally, H.J., Banerdt, W.B., Duxbury, T.H., 1998. Observations of the north polar region of Mars from the Mars Orbiter Laser Altimeter. Science 282, 2053–2060.